Research Square

Preprints are preliminary reports that have not undergone peer review. They should not be considered conclusive, used to inform clinical practice, or referenced by the media as validated information.

A hybrid model using data mining and multi-criteria decision-making methods for landslide risk mapping at Golestan Province, Iran

Elham Rafiei Sardooi
University of Jiroft
Ali Azareh (aliazareh@ujiroft.ac.ir)
University of Jiroft
Tayyebeh Mesbahzadeh
University of Tehran
Farshad Soleimani Sardoo
University of Jiroft
Eric J. R. Parteli
University of Duisburg Essen - Campus Duisburg: Universitat Duisburg-Essen
Biswajeet Pradhan
University of Technology Sydney

Research Article

Keywords: landslide, hazard, vulnerability, risk, GIS

Posted Date: July 6th, 2021

DOI: https://doi.org/10.21203/rs.3.rs-190817/v1

License: This work is licensed under a Creative Commons Attribution 4.0 International License.
Read Full License

Version of Record: A version of this preprint was published at Environmental Earth Sciences on July 21st, 2021. See the published version at https://doi.org/10.1007/s12665-021-09788-z.

A hybrid model using data mining and multi-criteria decision-making methods for landslide risk mapping at Golestan Province, Iran

Elham Rafiei Sardooi[1]*, Ali Azareh[2]*, Tayyebeh Mesbahzadeh[3], Farshad Soleimani Sardoo[4], Eric J. R. Parteli[5], Biswajeet Pradhan[6,7]

1. *Department of Ecological Engineering, Faculty of Natural Recourses, University of Jiroft, Kerman, Iran, Corresponding author: ellrafiei@ujiroft.ac.ir
2. * Department of Geography, University of Jiroft, Kerman, Iran, Corresponding author: aliazareh@ujiroft.ac.ir
3. Department of Reclamation of Arid and Mountain Regions, Faculty of Natural Resources, University of Tehran, Tehran, Iran, tmesbah@ut.ac.ir
4. Department of Ecological Engineering, Faculty of Natural Recourses, University of Jiroft, Kerman, Iran, f.soleimani@ujiroft.ac.ir
5. Faculty of Physics, University of Duisburg-Essen, 47057 Duisburg, Germany, eric.parteli@uni-due.de.
6. The Centre for Advanced Modelling and Geospatial Information Systems (CAMGIS), Faculty of Engineering & IT, University of Technology Sydney, Ultimo 2007, New South Wales, Australia, Biswajeet.Pradhan@uts.edu.au
7. Department of Energy and Mineral Resources Engineering, Sejong University, Choongmu-gwan, 209, Neungdong-ro, Gwangin-gu, Seoul 05006, Korea; biswajeet24@gmail.com

Abstract

The accurate modelling of landslide risk is essential pre-requisite for the development of reliable landslide control and mitigation strategies. However, landslide risk depends on the poorly known environmental and socio-economic factors for regional patterns of landslide occurrence probability and vulnerability, which constitute still a matter of research. Here, a hybrid model is described that couples data mining and multi-criteria decision-making methods for hazard and vulnerability mapping and presents its application to landslide risk assessment in Golestan Province, Northeastern Iran. To this end, landslide probability is mapped using three state-of-the-art machine learning (ML) algorithms – Maximum Entropy, Support Vector Machine and Genetic Algorithm for Rule Set Production – and combine the results with Fuzzy Analytical Hierarchy Process computations of vulnerability to obtain the landslide risk map. Based on obtained results, a discussion is presented on landslide probability as a function of the main relevant human-environmental conditioning factors in Golestan Province. In particular, from the response curves of the machine learning algorithms, it can be found that the probability p of landslide occurrence decreases nearly exponentially with the distance x to the next road, fault or river. Specifically, the results indicated that $p \approx \exp(-\lambda x)$, where the length-scale λ is about 0.0797 km^{-1} for road, 0.108 km^{-1} for fault and 0.734 km^{-1} for river. Furthermore, according to the results, p follows, approximately, a lognormal function of elevation, while the equation $p = p_0 - K \cdot (\theta - \theta_0)^2$ fits well the dependence of landslide modeling on the

slope-angle θ, with $p_0 \approx 0.64$, $\theta_0 \approx 25.6°$ and $|K| \approx 6.6 \times 10^{-4}$. However, the highest predicted landslide risk levels in Golestan Province are located in the south and southwest areas surrounding Gorgan City, owing to the combined effect of dense local human occupation and strongly landslide-prone environmental conditions. Obtained results provide insights for quantitative modelling of landslide risk, as well as for priority planning in landslide risk management.

Keywords: landslide; hazard; vulnerability; risk; GIS

1 Introduction

Landslides constitute one of the most hazardous natural phenomena, causing live losses and devastating impact on local infrastructure every year around the globe (e.g., Radbruch-Hall & Varnes 1976; Suzen and Doyuran, 2004a; Suzen and Doyuran, 2004b; van Westen et al. 2005; Guzzetti et al. 2012; Wang et al. 2019; Lato et al. 2019). The development of improved measures for landslide damage control and mitigation relies on the quantitative assessment of local landslide risk, i.e., the potential degree of personal and material loss due to the occurrence of damaging landslide events (Chacon et al. 2006; Glade and Crozier,2005a; Glade and Crozier,2005b; Glade et al. 2005; Guzzetti, 2005; Guzzetti et al. 2012; Varnes, 1984). However, this assessment is challenging due to the broad range of environmental and anthropogenic factors involved, and because the processes underlying landslide initiation and dynamics are still poorly understood (de Blasio, 2011; Shanmugam & Wang, 2015; Achour & Pourghasemi, 2020).

The first step toward a modeling framework for landslide risk assessment consists in estimating landslide-prone zones based on the landslide occurrence in the area. Therefore, a *landslide hazard map*, which characterizes the probability of landslide occurrence in a certain area under consideration of the main local and regional factors that potentially trigger landslides, is required. To this end, the various potential causative factors must be statistically evaluated against the background of a local inventory map, which encodes information on the areas affected by damaging landslides (Brabb, 1985).

The last decade has witnessed much progress in the modelling of landslide hazard maps, in particular owing to recent advances in artificial intelligence and its application to remote sensing and geoscientific research (Yesilnacar & Topal 2005; Pradhan et al. 2010; Erener & Düzgün 2012; Kornejady et al. 2017; Mirzaei et al. 2018; Chen et al. 2017a; Pandey et al. 2020; Vakhshoori et al. 2019). For instance, GIS-based multi-criteria decision-making approaches, such as Fuzzy Analytic Hierarchy Process (FAHP), have been applied to identifying areas susceptible to damaging landslides (Ercanoglu & Gokceoglu 2002; Gorsevski et al. 2006; Gorsevski & Jankowski 2010; Vahidnia et al. 2010; Pourghasemi et al. 2012; Feizizadeh et al. 2013; Tazik et al.

2014; Roodposhti et al. 2014; Feizizadeh et al. 2014; Zhao et al. 2017; El Bcharia et al. 2019; Roy & Saha, 2019). Moreover, various machine learning algorithms, including support vector machine (SVM) (Pourghasemi & Kerle 2016; Youssef et al. 2016; Pandy et al. 2018), Maximum Entropy (MaxEnt) (Park, 2015; Kornejady et al. 2017; Pandy et al. 2018; Mokhtari & Abedian, 2019), Genetic Algorithm Rule-Set Production (GARP) 2015; (Stockwell, 1999; Rahmati et al. 2019; Adineh et al. 2018) and Random forest (RF) (Goetz et al. Pourghasemi & Kerle 2016; Sevgen et al. 2019; Pourghasemi et al. 2020), and also, deep learning techniques including recurrent neural network (RNN) and Convolution Neural Networks (CNN) (Xiao et al. 2018; Ghorbanzadeh et al. 2019; Mohan et al. 2020; Bui et al. 2020; Ngo et al. 2021) have been applied to assessing landslide hazard within a broad range of geographical locations and conditions of soil type, topography, land use/land cover, climate and anthropogenic influences (for a recent discussion, see Achour and Pourghasemi, 2020). However, the performance of the different algorithms in the computation of spatial landslide probability distribution is still poorly known. More precisely, as shown in previous studies, the GARP algorithm has good performance in spatial modeling (Stockman et al. 2006; Sánchez-Flores, 2007; Wang et al. 2010; Adineh et al. 2018). However, this model has been rarely used in landslide studies. Furthermore, the SVM and MAXENT models have performed very well in spatial prediction of landslides (Park, 2015; Kornejady et al. 2017; Chen et al. 2017a; Kalantar et al. 2018). Therefore, it is pertinent to evaluate the applicability of these models in the context of hazard and vulnerability maps.

Furthermore, the landslide hazard map must be combined with information on the level of damage associated with a landslide of a certain type. Specifically, an additional map – the *landslide vulnerability map* – which describes the potential landslide damage on local population, property, infrastructure, and public services, is required. This vulnerability map constitutes the second step toward landslide risk assessment (Guillard-Gonçalves & Zêzere 2018). By suitably combining the vulnerability map with the hazard map, a *landslide risk map* can be obtained, which provides a joint probabilistic assessment of damaging landslide occurrence and the concatenated socio-economic impacts (Frigerio & Amicis, 2016; Murillo-García et al. 2017; Guillard-Gonçalves & Zêzere, 2018).

However, landslide vulnerability mapping constitutes a challenging field of work given its intrinsic social, environmental, and economical facets. Specifically, both physical vulnerability (i.e., the potential degree of damage caused to physical components such as buildings, infrastructure, etc.) and social vulnerability must be modeled. Indeed, the concept of social vulnerability refers, in a broad sense, to personal injuries and impact of a damaging landslide on different socio-economical groups, but still lacks common definition (Guillard-Gonçalves & Zêzere, 2018). Furthermore, various aspects of social vulnerability relate to potential material losses in the private and public sectors as well, and it is, thus, difficult to mathematically treating social vulnerability by excluding the physical aspect of vulnerability.

In the present work, a new method is presented for landslide risk assessment and its application to Golestan Province in Iran (Fig. 1). This method integrates data mining and decision-making methods, which have received less attention in previous studies of landslide, to estimate the regional hazard and vulnerability maps, under consideration of the local landslide inventory, as well as all main relevant human-environmental factors, as described next. Subsequently, the landslide risk map is obtained by combining the hazard and vulnerability maps, which allows us to identify and characterize high-risk landslide areas in Golestan Province. Specifically,

2 Factors for landslide hazard and vulnerability in the study area

Golestan Province lies in Northeastern Iran, within latitude ranges from $36^{\circ}27'48''$ N to $38^{\circ}14'56''$ N, and longitude ranges from $53^{\circ}40'29''$ E to $56^{\circ}30'44''$ E (Fig. 1). It has an area of 20347 km^2, which comprises 1.3% of Iran’s territory. Data on landslide positions (440 points) within Golestan Province are available from the Geological Survey and Mineral Explorations of Iran (GSI). These data were processed using Google Earth images and field surveys, which led to the spatial distribution of landslide events is shown in Fig. 1. Moreover, images of landslides within the study area have indicated in Fig. 2.

We remark that one constraint in the type of spatial analysis performed in our work is that the maps associated with the different input factors are available at distinct scales. This constraint is indeed common to the type of study considered here, i.e., it is an inevitable constraint in environmental research and is related to *limitations* on *data availability* (Mosavi et al. 2020), as discussed thoroughly in preceding work (Pourghasemi et al. 2013; Hong et al. 2016; Mokhtari and Abedian, 2019; Mosavi et al. 2020). However, the solution to this constraint consists in resampling the input variables to the same spatial resolution, which is what we have done in the present work. By suitably rescaling the input data sets, the computation of the landslide hazard maps in developing countries can provide a helpful tool in land degradation research.

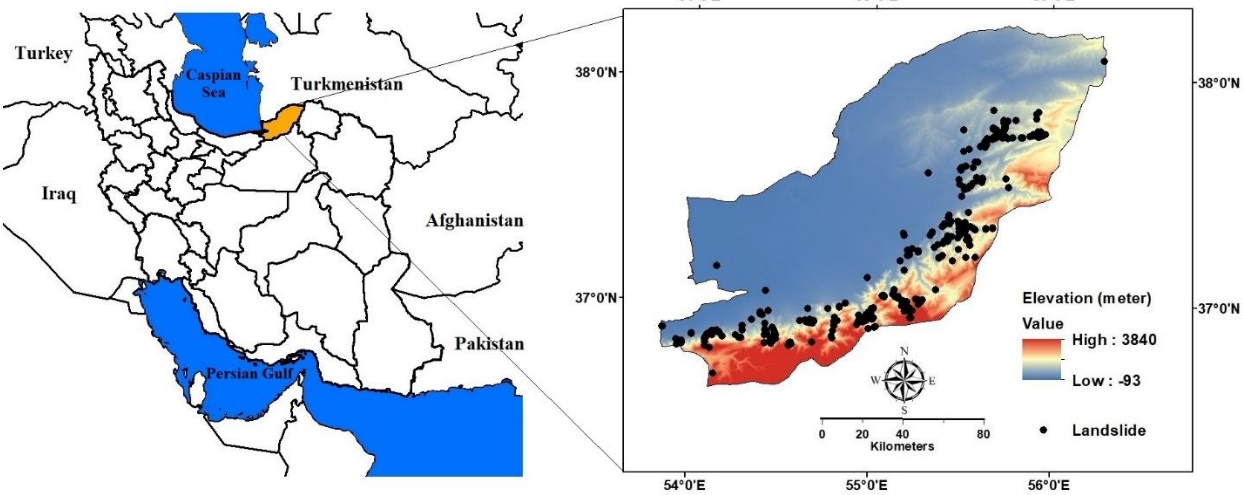

Fig. 1. Location of the study area, Golestan Province, Iran. The dots on the elevation map (right) denote landslide occurrence locations obtained from the Geological Survey and Mineral Explorations of Iran (GSI).

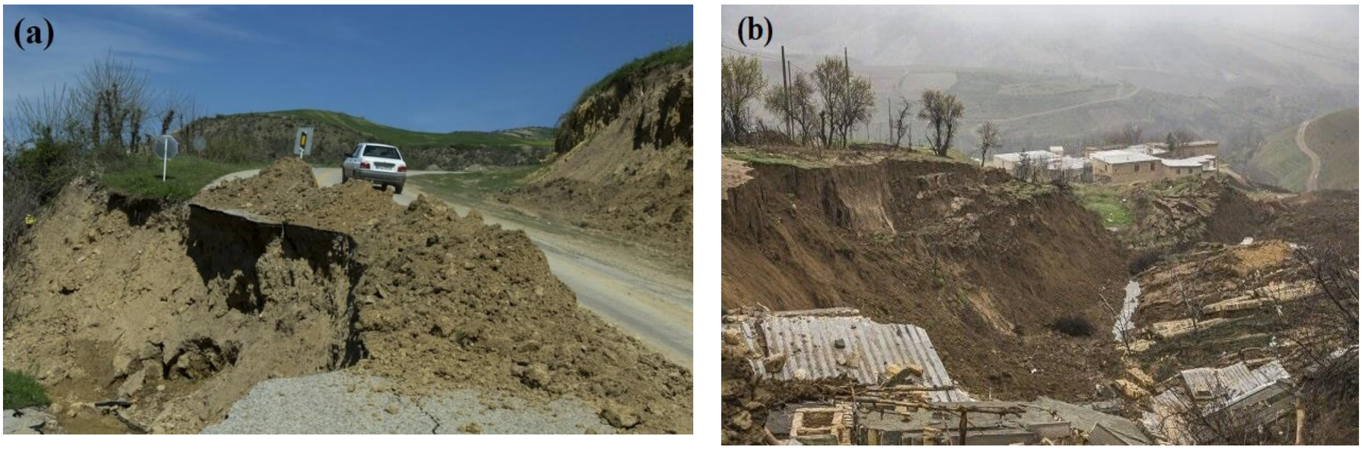

Fig. 2. Images of landslides within the study area (retrieved from Mehrnews, 2020).

Various factors compete to rendering the study area of the present work potentially prone to damaging landslide events. The average annual rainfall of Golestan Province ranges from 200 mm to 1000 mm. There is a significant relationship between elevation and rainfall (Dhurmea et al. 2009). Since the elevation of the study area ranges from -93 meters (below the average sea level) in coastal regions to 3840 meters asl (above the average sea level) in southern regions, as a result, rainfall changes in the study area are high. The local geology of the study area consists of limestones of the Lar and Mozdoran Formation (upper Jurassic age), Quaternary sediment types (Qm and Qsw), shales of the Sanganeh Formation (Early Cretaceous) and shale and sandstone of the Shemshak Formation (Triassic-Jurassic). Furthermore, nonprincipled criteria for road construction and land use/land cover adopted in Golestan Province are some of the human influences affecting landslide hazard in the area.

In particular, forest prevails in the southern and eastern regions, while agriculture and pasture represent the main types of land use/land cover elsewhere. However, the relevance of the various factors for the spatial distribution of landslides is poorly known. In the following subsection, the various landslide hazard factors are described based on GIS and statistical data sets available for Golestan Province. Subsequently, the social-economic factors controlling landslide vulnerability are specified and discussed. Figure. 3. indicates the methodological flowchart of this study.

According to flowchart, the major steps of this study are: (1) comparing the machine learning methods of Genetic Algorithm for Rule Set Production (GARP), Support Vector Machine (SVM) and Maximum Entropy (MaxEnt) to predict landslide hazard maps, (2) assessing the landslide conditioning factors and the determination of the most important factors, (3) creating landslide vulnerability map based on the analytic hierarchy process (AHP) approach, (4) integrating the best machine learning method with MCDM approaches to create landslide risk map and to characterize the high landslide risk regions.

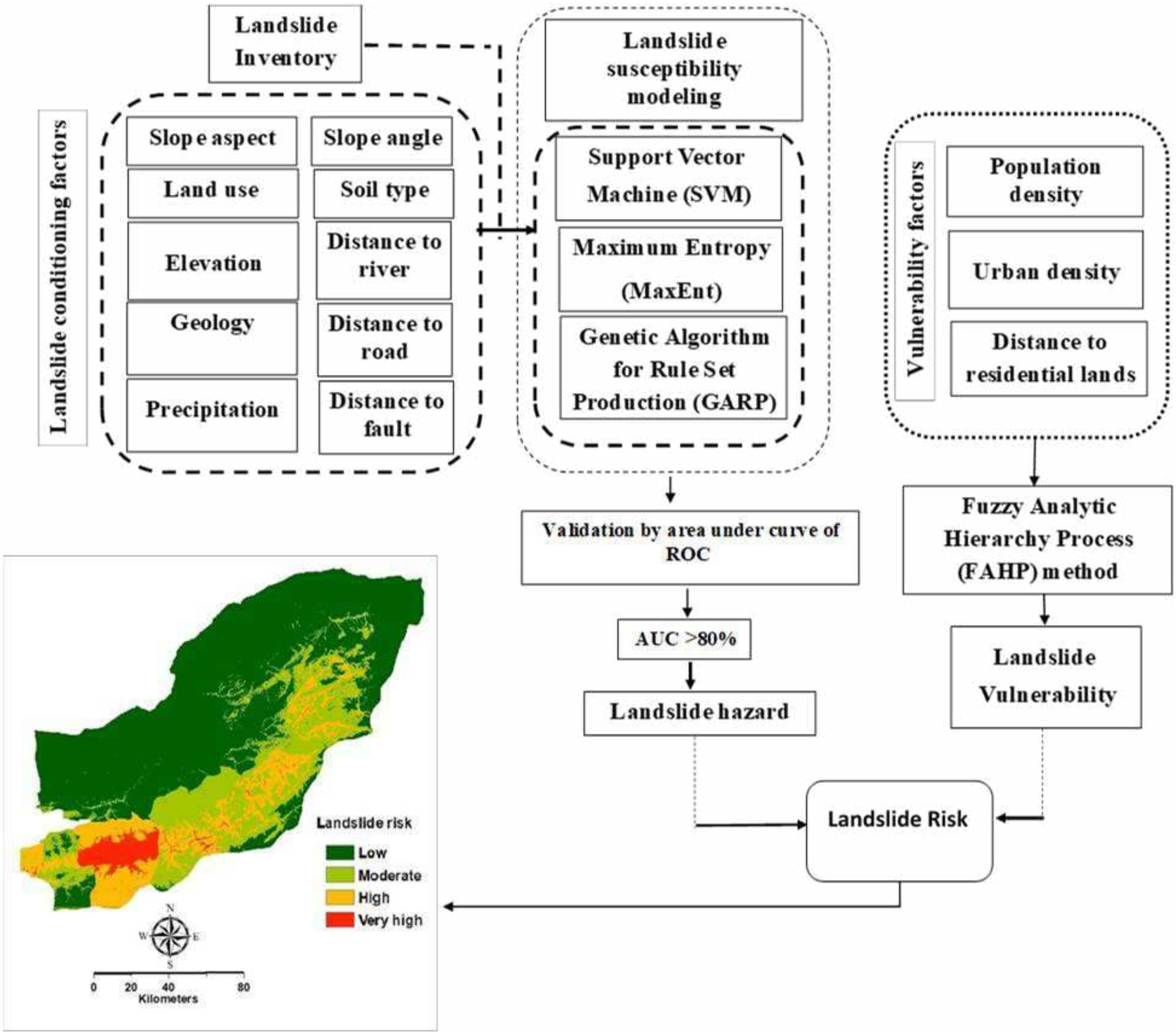

Fig. 3. The methodological flowchart of the present study

2.1 Landslide hazard factors

To calculate the landslide hazard map for Golestan Province, we follow Ashournejad et al. (2019) and consider the following main two-dimensional fields: Digital Elevation Model (DEM), soil type, slope-aspect, slope-angle, geology, distance to fault, land use/land cover (LULC), distance to road, distance to the river and precipitation. The characteristics of these factors in Golestan Province are described below.

We note that the maps associated with the factors considered in the study area are not available all at the same scale. However, we have resampled all maps using the same cell size (30 meter) in ArcGIS, thus allowing us to overlay the various maps. This scenario resembles, indeed, the situation encountered in previous work, in which data sets associated with different spatial scales were considered for the computation of hazard maps associated with landslide and other environmental studies (Adineh et al. 2018; Pourgahsemi & Kerle, 2016).

2.1.1 Slope-aspect

Slope-aspect affects local solar radiation and vegetation growth, and has been thus pointed out as important and effective factor for landslides (Sidle & Ochiai, 2006; Kumar & Anbalagan, 2015). Golestan Province hosts a mountainous terrain which leads to potentially relevant spatial variability in slope-aspect. Thus, slope-aspect was considered as potential factor for landslide hazard in Golestan Province. Figure. 4a displays the corresponding slope-aspect map, prepared and classified on DEM with a cell size of 30 m × 30 m in ArcGIS 10.2.2.

2.1.2 Slope-angle

Moreover, the angle between the sloping side of a granular soil and the horizontal – i.e., the slope-angle – is one of the most important parameters for landslide initiation. Wherever this angle exceeds the soil's angle of maximal stability against gravitational stresses, the surface relaxes through avalanches in the direction of steepest descent, thus triggering a landslide (see, e.g., Beakawi Al-Hashemi and Baghabra Al-Amoudi, 2018). However, this angle of maximal stability, also called angle of repose, depends on frictional and cohesive inter-particle forces that follow a still poorly known function of various factors, such as particle size distribution, degree of consolidation, moisture content, particle shape and material (Parteli et al., 2014; Schmidt et al., 2020). Moreover, the modeling of landslide initiation processes and the role of slope-angle must consider whether the soil is cohesive or not, and whether the soil is constituted of consolidated materials or rocks. The relationship between the probability of landslide occurrence and slope-angle is still uncertain (Neuhauser & Terhorst, 2007; Dymond et al. 2006; Demir et al., 2013). In the present work, the slope-angle map was generated for Golestan Province based on the DEM in ArcGIS 10.2.2. Figure. 4b shows that the slope-angle ranges from about 0° degrees in the north to approximately 71° degrees within the south and east areas of Golestan Province.

2.1.3 Precipitation

As shown in previous work, the local landslide occurrence probability is strongly correlated with rainfall (Kawagoe et al. 2010; Althuwaynee et al. 2015). Infiltration and runoff enhance soil instability and saturation levels, raindrop impacts on sloping granular surfaces constitute an important mechanism of downhill sediment transport, and rainfall-induced processes may increase landslide hazard over multiple time-scales, for instance by affecting moisture content and increasing local slope instability (Hong et al. 2006). In the present work, the precipitation map of Golestan Province (Fig. 4c) has been calculated based on annual average precipitation data of 33 rain gauge stations from the Iran Meteorological Organization. According to Fig. 4c, the amount of precipitation ranges from 200 mm near the borders of coastal regions to 1000 mm near the central region of Golestan Province (Fig. 4c).

It should be noted that the intensity and variation of rainfall are important aspects in the statistics, in addition to the mean rainfall. However, recording rain gauge stations and hourly rainfall data would be needed to estimate the intensity of rainfall. In the study area, the number of recording rain gauge stations (with hourly data) was limited, so that the analysis of the present work relies on the average rainfall data based on the statistics of rain gauge stations. Therefore, the present study can be compared to previous work, in which the conditioning factor associated with rainfall was based on average precipitation data (Aghdam et al., 2017).

2.1.4 Distance to river

There are three main and consistent rivers in Golestan Province, namely Gorgan River, Qarasu and Atrak rivers (they are not valleys or streams). Distance to the river may affect landslide hazard, as groundwater flow toward rivers and water rivers provides an effective mechanism for soil undercutting (Korup et al. 2007; Tang et al. 2011; Zaruba and Mencl 2014). Previous work has shown that landslides occur often along river sides, and that the proximity to rivers underwashes hillside slope foot by flood, thus further enhancing landslide hazard (Dai et al., 2001). Figure 4d shows the spatial distribution of distance to the river for Golestan Province, obtained with ArcGIS 10.2.2.

2.1.5 Land use/Land cover

Land use/land cover has an impact on soil properties, geology and land cover dynamics, and represents one major factor for enhancing rainfall-driven landslide occurrence. Human activities of various types are well-known cause of vegetation cover reduction and increased soil instability, and favor gully and runoff erosion (Fell et al. 2008; Karsli et al. 2009). Moreover, forest, orchard, rangeland and agricultural lands stand for the land use/land cover practices with highest impact on landslide occurrence (Ercanoglu & Gokceoglu, 2004). For instance, agricultural and orchard land use/land cover affect soil mechanics through irrigation processes and alterations in natural vegetation cover, while forest practices further increase landslide hazard wherever land use/land cover is inappropriate, especially near roads (see below). Landsat Operational Land Imager (OLI) images (Landsat 8) was used to extract the 2019 land use/land cover map for Golestan Province. The supervised classification method of Maximum Likelihood (ML) was used in ENVI 5.1 software to provide the land use/land cover maps. Finally, land use/land cover map of the study area was classified into six classes including: urban, bare land, rangeland, forest, orchard and agriculture (Fig. 4e).

2.1.6 Elevation

Elevation is another important factor for landslide occurrence, since at higher altitudes various phenomena compete to favor soil instability processes, such as snowmelt, sparse vegetation, enhanced rock weathering and rainfall (Pachauri, 1998; Dai & Lee, 2002; Catani et al., 2013). Figure. 4f shows the Digital Elevation Model (DEM 30 meter) of Golestan Province, which has been obtained from topographic maps in 1:25000 scale prepared by Department of Water Resources Management of Iran (DWRMI). The preparation of DEM map based on topography map was done in ArcGIS 10.2.2 using "Topo to raster" command. According to Fig. 4f, the elevation of the study area ranges from -93 meters (below the average sea level) in coastal regions to 3840 meters asl (above the average sea level) in southern regions. Specifically, negative values of elevation (Z) mean that the Z is below a reference value (Z= 0) associated with sea level. Persian Gulf is the base level for measuring elevation in Iran. Elevation in coastal region was -93 meters below the average sea level.

2.1.7 Distance to fault

Fault dynamics cause rock displacement, avalanches, seams and cracks on the soil, thus constituting one major cause for slope instability (Pham et al. 2018). Landslide occurrence in areas affected by tectonic processes and seismic activity tends, thus, to increase with proximity to fault. By means of field investigation and remote sensing, a negative exponential scaling was proposed to quantitatively predict the number of earthquake-triggered landslides per unit area as a function of the distance to the causative fault (Zhuang et al., 2010). However, this quantification is difficult because landslide hazard depends on the interplay between prevailing seismic modes, perturbation magnitude, fore- and aftershock dynamics and the other local environmental factors causative of landslides.

The study area is placed in Northeast Iran, north of the Eastern Alborz Mountains and east of the South Caspian block and its lithology consists of limestone, Quaternary sediment types, shales and sandstones. The Khazar and North Alborz fault zones are the most important faults of the study area. One of the important active fault zones located in the Golestan province is the Khazar fault zone, including Minoodasht, Behshahr, Sari, and Amol faults

(Tourani et al. 2021). According to previous studies, the thrusting of the Alborz Mountains towards the south of the Southern Caspian block occurs along the Khazar fault zone (Axen et al. 2001 and Allen et al. 2003). The active Khazar fault zone indicates reverse/thrust fault properties and has created many significant earthquakes during the instrumental period (Tourani et al. 2021).

Figure. 4g shows the two-dimensional field associated with local distance to the next fault within Golestan Province, which it has been obtained using ArcGIS 10.2.2.

2.1.8 Lithology

Lithology, i.e., the type of rock constituting the soil, affects landslide hazard because some types of rock are more affected by degradation resulting from water infiltration than others. However, the relationship between lithology, rock degradation and soil instability is poorly understood. Different geological formations in the Golestan Province, such as limestone, gypsum, shale and sandstone, which are particularly prone to infiltration-induced degradation, occur in areas of high density of landslides (Fig. 4h). Furthermore, there are Quaternary sediments including Qm and Qsw, along the margins of the Caspian Sea. Swamp deposits (Qsw) include gray to brown, silty, clayey, gravelly sand covered by organic rich, fine to coarse sand and silt. Swamp deposits are found in the upper reaches of the modern stream valleys, along the margins of the Caspian Sea, and in poorly-drained areas on the uplands. Along the margins of the Caspian Sea, swamp deposits are up to 15 ft thick and have several feet of organic silt near the land surface. March deposits (Qm) include light-gray to brown, organic-rich, clayey silt. These deposits are located along the margins of the Caspian Sea. In general, the thickness of marsh deposits is less than 10 ft. Table 1 lists the main classes of lithology in Golestan Province.

Table 1. Lithology classes in the study area.

Code	Lithology	Formation	Geological age
Qm	Marsh deposits	-	Quaternary
Ksn	Grey to block shale and thin layers of siltstone and sandstone	Sanganeh	Early Cretaceous
Qsw	Swamp deposits	-	Quaternary
DCkh	Limestone, locally including gypsum	Lar & Mozdoran	Jurassic
TRJs	Dark grey shale and sandstone	Shemshak	Triassic-Jurassic

2.1.9 Soil type

Soil type constitutes one main property for hillslope instability. Fine-grained soils, in particular, are less permeable and more prone to landslides than coarse-grain soils (Lepore et al. 2012; Alkhasawneh et al. 2014), while material properties and particle chemistry further affect inter-particle frictional forces and soil flowability. Following USDA soil taxonomy, soil types in Golestan Province can be classified into the following categories:

- alfisol – rich in iron, aluminum, moisture and clay
- aridisol – dry, poor in organic matter, characterized by slow formation rates
- entisol – unconsolidated sediments, in particular sand, clay or volcanic ash
- inceptisol – young soils with poorly developed vertical profile
- mollisol – deep, fertile soils of soft texture characterizing grasslands

The spatial distribution of the prevailing soil type in Golestan Province is shown in Fig. 4i. It should be noted that soil type and lithology constitute distinct environmental factors, and there is a significant relationship between these factors with landslide hazard based on Jackknif test, as shown later in this manuscript. There, it is necessary to use both factors. We refer to previous work (Van Den Eeckhaut et al. 2012 and Mohammady et al. 2012) which has used both factors for modeling landslide hazard, such as in the present study.

2.1.10 Distance to road

Regions within higher proximity to roads are more prone to landslide occurrence due to undercutting- and overloading-driven processes of mechanical hillslope destabilization (Duman et al. 2006, Lee, 2007, Yalcin, 2008). The effect of roads on landslide hazard is tendentially stronger in developing countries owing to inadequate drainage system, which further contributes to enhance soil instability. As shown in previous work (Brenning et al., 2015), landslide hazard near highways may be increased by one order of magnitude, both owing to mechanical stresses on the base of hillslopes and to the contribution of further types of human interference in nearby areas, such as grazing. Moreover, roads cause vertical cuts that increase the pressure on their lower part, thus further enhancing landslide hazard. Figure. 4j shows the spatial distribution of distance to the road in Golestan Province.

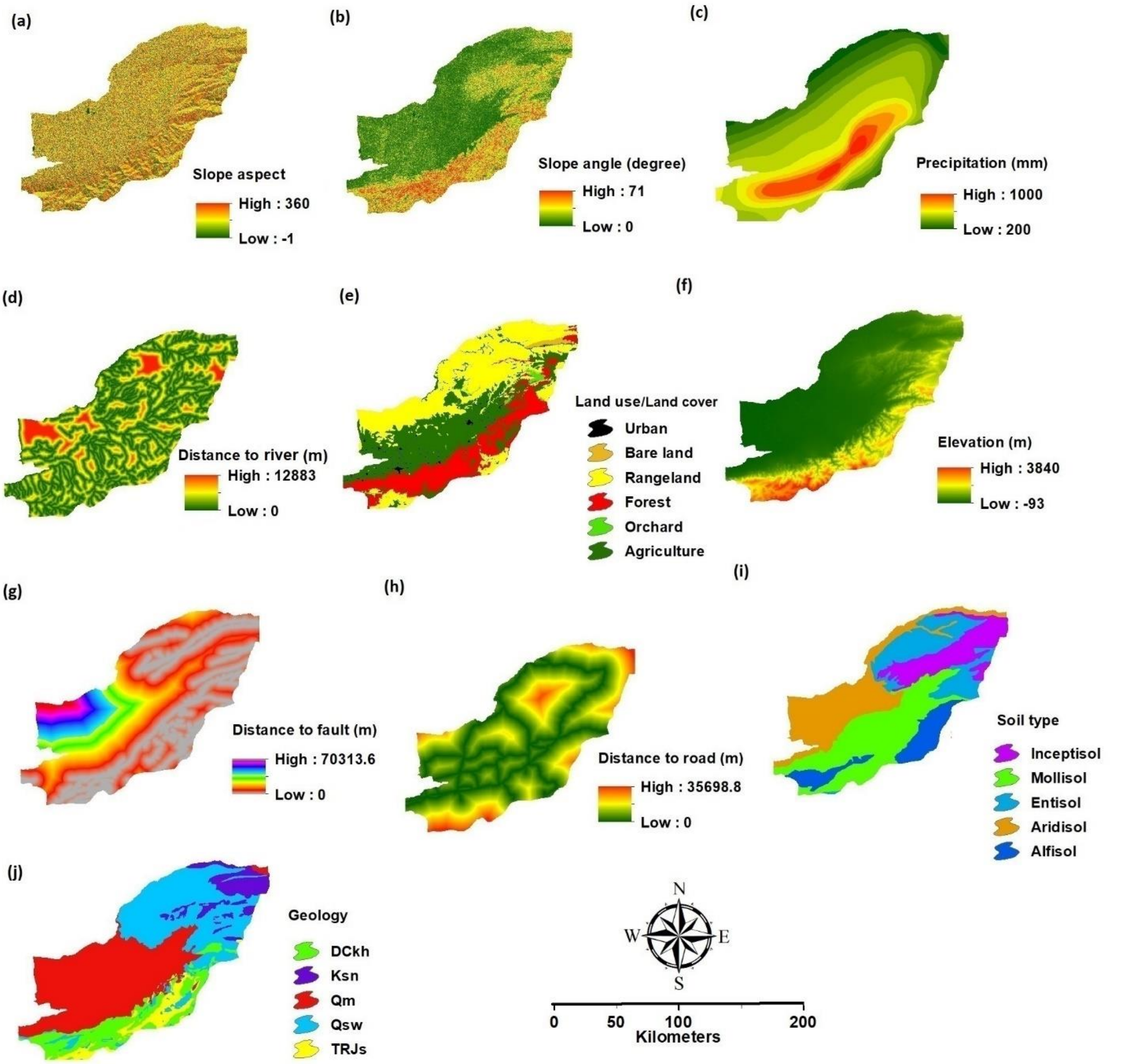

Fig. 4. Spatial distribution of the main landslide hazard factors in Golestan Province: a) slope-aspect, b) slope-angle, c) precipitation, d) distance to river, e) land use/ land cover, f) elevation g) distance to fault, h) distance to road, i) soil type, and j) lithology.

2.2 Landslide vulnerability factors

Vulnerability refers to the potential level of devastation caused by a natural hazard of a certain type to society, infrastructure and properties (Tobin & Montz, 1997). However, vulnerability has no standard definition and must be characterized under consideration of the type of natural hazard and the various aspects associated with the human-environmental setting that are relevant for damage characterization. Following considerations of previous work (Murillo-García et al. 2017; Guillard-Gonçalves & Zêzere, 2018), finally, the following landslide vulnerability factors within Golestan Province were identified: urban population density, urban building density and distance from urban areas to landslide locations (discussed below).

Indeed, the maps associated with the landslide vulnerability factors in the study region are not available all at the same scale. We share, thus, the challenge met by different authors in previous work dealing with diverse maps, each with a distinct spatial resolution (Adineh et al. 2018; Pourgahsemi & Kerle, 2016). In the present work, we have resampled all maps based on the same cell size (30 meter) in ArcGIS, so that the analysis has been performed using this spatial resolution.

2.2.1 Urban population density

Urban population density is defined as the number of individuals per unit area residing in an urban region. The larger the population density, the larger the number of individuals subjected to a local damaging landslide, and the higher, thus, the social vulnerability (Cutter et al. 2003; Uzielli et al. 2008; Kjekstad & Highland; 2009, Murillo-García et al. 2015). We noted that additional social aspects, such as population distribution and social-economic development, may further affect, to some extent, local landslide vulnerability. However, given that political and cultural influences do not vary much within Golestan Province, it is reasonable to regard population density as the main causative factor for social vulnerability in the study area. Population density in Golestan Province was classified as specified in Fig. 5a and table 2 (data from Iran Statistical Center Organization, 2016).

Table2. Population density in different cities of Golestan Province

City	Population	Area(km^2)	Urban population density (person/km2)
Gorgan	480541	1578	305
Gonbad-e Qavus	348744	4996	70
Aliabad-e Katul	140709	1100	128
Aqqala	132733	1842	72
Kalaleh	117319	1863	63
Azadshahr	96803	848	114
Ramian	86210	827	104
Bandar-e Torkaman	79978	283	283
Minudasht	75483	663	114
Kordkuy	71270	856	83
Gomishan	68773	1281	54
Galikash	63173	868	73
Maraveh Tappeh	60953	3097	20
Bandar-e Gaz	46130	246	187
Total	1868819	20347	92

2.2.2 Urban building density

Urban building density – the number of buildings per unit area within an urban region – is one major factor for physical vulnerability. We noted that this vulnerability incorporates potential damage to any physical component of the private and public sectors, including building distribution. However, if we assume that public-infra structure and private property represent potential development indicators in Golestan Province, and that these indicators are correlated with each other to some extent, then it is plausible to adopt urban building density as one quantitative measure for socio-economic development – and vulnerability. Figure. 5b shows the building density map for the study area (data available from Iran Statistical Center Organization, 2016).

2.2.3 Distance from urban area to next landslide location

Because frictional forces cause energy dissipation thus counteracting the sediment transport processes, landslide vulnerability tends to decrease with distance to landslide areas. By contrast, the closer an urban area is to a landslide location, the higher the potential level of damage associated with an event of a certain type. Figure. 5c shows the two-dimensional field corresponding to the distance between the urban regions and landslide locations, obtained from the Digital Elevation Model of Golestan Province. We noted interurban infra-structure such as roads and railway could be also incorporated into Fig. 5c, but have not been included in this map given that they depend on the spatial distribution of urban areas and further reflect regional levels of socio-economic development that have been already considered in Sections 2.2.1. Therefore, vulnerability factors considered above incorporate all main aspects controlling potential socio-economic damage of landslides and are, thus, applied for landslide risk mapping as described next.

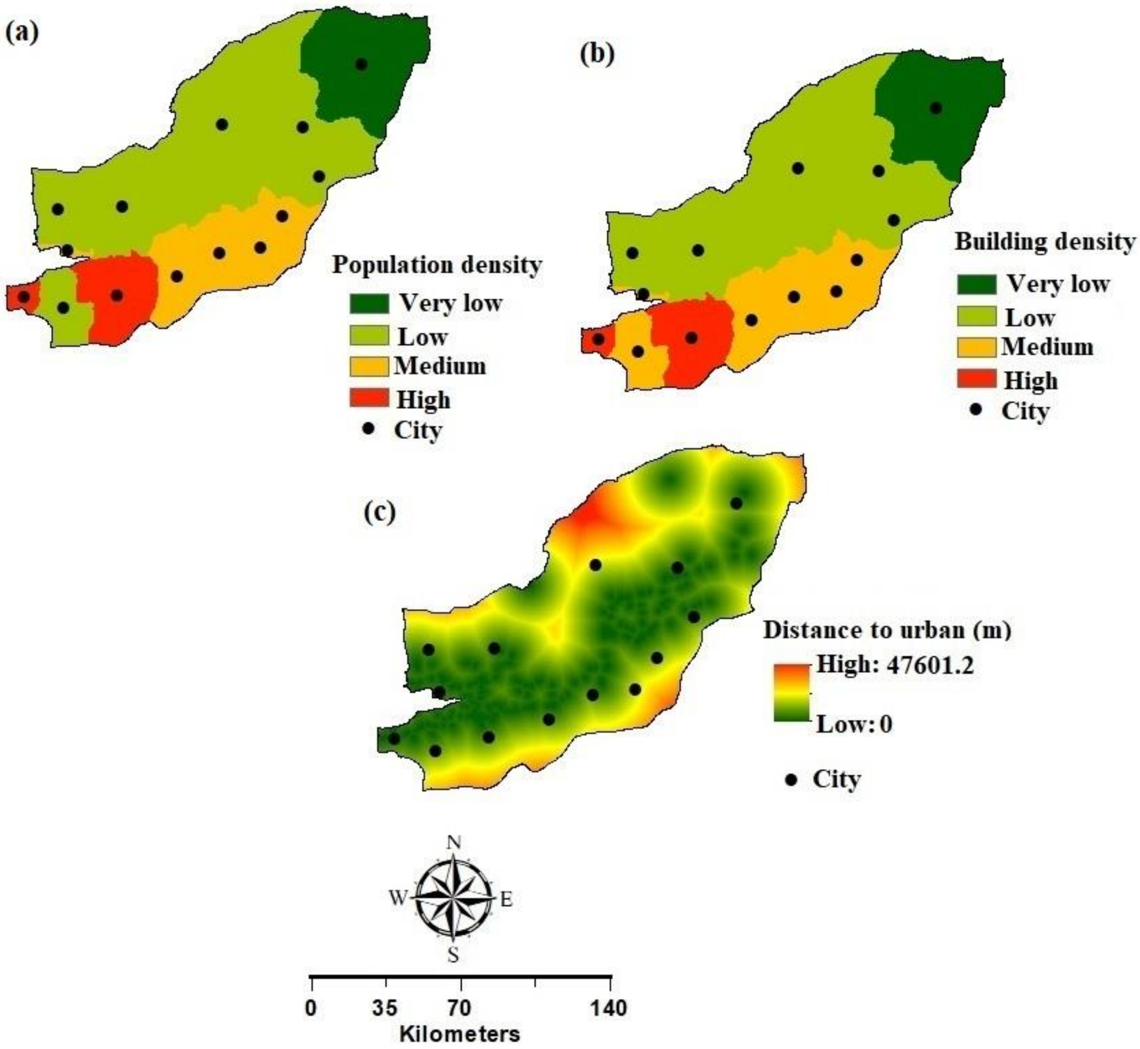

Fig. 5. Spatial distribution of the main landslide vulnerability factors: a) urban population density, b) urban landslide density, and c) distance from urban area to landslide location.

3 Calculation of the landslide hazard, vulnerability and risk maps

Machine learning algorithms were applied to calculate hazard, vulnerability and risk maps based on the data sets described in the previous section, as well as the landslide inventory map shown in Fig. 1. To this end, the positions in the inventory map associated with the 440 landslide events were divided into two groups: Training data, corresponding to randomly chosen 70% of the landslide positions, and test data, comprising 30% of the corresponding data set (Pourghasemi et al. 2013; Adineh et al. 2018). Specifically, the first group was employed in the search for correlation patterns between spatial distributions of landslide events, hazard factors and vulnerability factors, while the second group was used for testing the obtained relationships in the framework of machine learning (Hastie et al., 2017). Based on these relationships, the maps for landslide hazard and vulnerability were computed, whereupon a landslide risk map for Golestan Province was obtained as described in the following subsections.

3.1 Landslide hazard map using Support Vector Machine, Maximum Entropy and Genetic Algorithm for Rule Set Production

To obtain the hazard map, we employed and compared the performance of three different machine learning algorithms for modelling landslide occurrence probability as a function of the conditioning factors specified in Section 2.1. These methods are described in Sections 3.1.1 – 3.1.3.

3.1.1 Support Vector Machine (SVM)

Support Vector Machine (SVM) stands for a learning-based data classification method (Vapnik, 1999; Yao et al., 2008; Peng et al., 2014). In the present work, SVM was applied for the first time to compute the hazard map for the entire Golestan province area. The goal is to divide the study area in classes of landslide hazard (from low to very high) based on the landslide inventory map and conditioning variables. More precisely, SVM assigns to each observed landslide location within the training data set one vector in the two-dimensional space, which is then classified according to a *local hazard level*, which is determined by the values of all hazard factors at the corresponding landslide location. Subsequently, the hazard map is computed by subdividing the study area into classes (clusters) of landslide hazard, each indicating a specific hazard level on the map. The border lines that separate neighboring classes on the map, which are called hyperplanes. The optimal hyper-plane maximizes the margin to divide the two categories, e.g., landslide and non-landslide. SVM has this name because each hyperplane is modeled using linear fitting functions determined from the vectors that lie nearest to it – these vectors are known as support vectors in the algorithm (e.g., Vapnik, 1999). The optimal hyper-plane can be determined based on the solution of optimization problem as follows (Samui, 2008):

$$\begin{aligned} &Minimize \sum_{i=1}^{n} \alpha_i - \frac{1}{2} \sum_{i=1}^{n} \sum_{j=1}^{n} \alpha_i \alpha_j y_i y_j (x_i x_j) \\ &if \quad \sum_{i=1}^{n} \alpha_i y_j = 0 \; and \;\; 0 \le \alpha_i \le C \end{aligned} \qquad (1)$$

where x is a vector of input space which includes selected conditioning factors, y is a training vector, C and α_i are the penalty factor and lagrange multipliers, respectively.

The training vectors consist of two categories (landslide and non-landslide pixels) are specified by two classes -1 and +1, respectively. The SVM method searches for an optimal hyper-plane which can recognize these two categories from these training vectors (Samui, 2008).

However, due to non-linearity effects inherent to natural systems, prior to applying classification the domain is often linearized by means of (kernel) functions. Specifically, the training vectors are mapped into a higher-dimensional space, in which computations can be performed using linear hyperplanes (Kecman, 2005; Hofmann et al. 2008; Marjanović et al. 2011; Ballabio & Sterlacchini, 2012; Chen et al. 2017a).

In this case, to classify the new dataset based on the SVM approach, the following decision function can be applied (Samui, 2008):

$$g(x) = sign\left(\sum_{i=1}^{n} y_i \alpha_i K(x_i x_j) + b\right) \qquad (2)$$

where $g(x)$ is decision function, b is a scalar base, $K(x_i x_j)$ is the kernel function,

Following previous work (Pourghasemi et al., 2013; Lee et al. 2017), we chose a Gaussian (bell-shaped) kernel function, which is also called Radial basis function (RBF) and has proven to deliver the best classification results in landslide hazard problems. This kernel function was determined using following equation (Vapnik, 1995):

$$K(x_i x_j) = e^{-\gamma (x_i - x_j)^2}, \gamma > 0 \qquad (3)$$

where γ is kernel width. The SVM model with RBF kernel available was run in openModeller Desktop 1.3.0 (de Souza Muñoz et al. 2011).

3.1.2 MaxEnt (Maximum Entropy)

MaxEnt is a data mining method to predict the occurrence of one event based on maximum entropy (Elith et al, 2011) that approximates the probability distribution of presence data based on environmental limitations (Phillips et al., 2006). In this model, the occurrence points (X_1 to X_m) are used to obtain an unknown probability distribution (Π) (Phillips et al. 2004; Phillips and Dudík, 2008; Kumar & Stohlgren, 2009) and the suitability of each pixel in the environment is expressed as a function of environmental variables. The maximum entropy model chooses a probability distribution that is near to reality and has entropy maximization (Phillips et al. 2006; Phillips et al. 2009; Felicísimo et al. 2013).

In this study, ME model was selected to predict landslide hazard. This model determines landslide occurrence probability distribution (π) in the set of positions X. The MaxEnt method has shown acceptable accuracy in the spatial modeling (Convertino et al. 2013; Chen et al. 2017b; Azareh et al. 2019). The objective occurrence probability at position x is expressed as (Phillips, 2008):

$$P(y=1/x)=\frac{P(y=1)P(x/y=1)}{P(x)}=\frac{P(y=1)\Pi(x)}{1/|x|} \quad (4)$$

where the probability of landslide occurrence is P(y = 1), while |x| is the number of pixels over the study area. Implementation was accomplished using the software MaxEnt 3.3.3 (Phillips et al., 2006).

3.1.3 Genetic Algorithm for Rule Set Production (GARP)

GARP is a data mining method based on a genetic algorithm designed to perform ecological modeling (Stockwell & Noble, 1992; Stockwell, 1999; Townsend Peterson et al. 2007; Adineh et al. 2018; Darabi et al. 2019). The algorithm was employed in previous spatial modelling (Stockman et al. 2006; Sánchez-Flores, 2007; Wang et al. 2010; Adineh et al. 2018), but its performance in regional landslide probability modelling is still uncertain.

A genetic algorithm starts with a large set of randomly generated competing solutions to a certain problem, which are refined over time to converge toward an optimal solution. Indeed, each solution can be regarded as a set ("chromosome") of models or parameter values ("genes"), which are iteratively refined by producing new sets of solutions. Moreover, in the framework of GARP, the solutions represent sets of environmental conditions, such as rainfall, elevation, climatic conditions, etc., which must be iteratively improved with regard to habitability by a given species on the basis of an inventory map for species occurrence (Stockwell, 1999; Townsend Peterson et al. 2007; Zhu et al. 2007; Wang et al. 2010; Boeckmann and Joyner, 2014; Adineh et al. 2018; Darabi et al. 2019).

In the problem of landslides investigated here, the landslide events stand for the species of the GARP algorithm, while the landslide inventory map constitutes the set of local observations that are needed to initialize the computations. The GARP model was run in openModeller Desktop 1.3.0 (de Souza Muñoz et al. 2011) to estimate the relationship (optimal solution) between spatial distribution of landslide occurrence and hazard factors, thus leading to the landslide hazard map.

3.2 Landslide vulnerability map using Fuzzy Analytical Hierarchical Process

A multi-criteria decision analysis technique was applied to evaluating local potential damage in Golestan Province, based on the landslide vulnerability factors identified in Section 2.2, i.e., urban population density, urban building density and distance to landslide location. Since the relative weights of these factors for the vulnerability map must be known, the method of Fuzzy Analytical Hierarchical Process (FAHP) was applied to estimate the combined effect of the respective spatial distributions.

Specifically, the FAHP method, has been described in detail in the literature (Saaty 1977; Carver 1991; Malczewski 1999; Ohta et al. 2007; Chen et al. 2016; Abay et al. 2019), discretizes the normalized values of each vulnerability factor to generate fuzzy variables, each allowing for 3 possible "membership" values: 0 (the minimum), 1 (the maximum) and an intermediate value reflecting the shape of the distribution. Each fuzzified vulnerability factor can take, thus, one of these membership values at a given location. Thereafter, the fuzzified factors are combined according to a weight vector, which encodes the relative influences (weights) of the different factors on the potential level of damage. Thus, a survey of local experts in the geology of Golestan Province was conducted to estimate the relative influences of the vulnerability factors of Section 2.2. Based on this information, in the framework of GARP, a comparison matrix encoding the weight ratio of all vulnerability factors is obtained and combined with the aforementioned fuzzy maps, thus leading weighted fuzzy maps (also called layers) associated with the different environmental and socio-economical variables. The final vulnerability map is obtained by overlaying the weighted fuzzy layers, which was accomplished here in the ARCGIS 10.2.2 environment.

It should be emphasized that the AHP-FUZZY method is used in our study, and not the pure AHP method. The AHP method determines the importance of variables only. However, in our work, each pixel was weighed and valued based on the fuzzy method, which was applied to the purpose of our work as described in Section 3. Furthermore, the importance of variables is determined entirely by decision-making methods and experts, and does not rely on any other method.

3.3 Landslide risk map

Interpretation of risk in the present work follows Schneiderbauer & Ehrlich (2004). Risk is a function of vulnerability and hazard (Glade and Crozier, 2005a; Glade and Crozier,2005b; Dewan, 2013). Therefore, local landslide risk is obtained here by combining the probability that a landslide occurs at a given location, under consideration of the conditioning factors (hazard), with the probability associated with a certain level of devastation caused by a damaging landslide (vulnerability). The landslide risk probability map for Golestan Province is obtained from the product of the landslide hazard and vulnerability maps, i.e., for every location, the local hazard is multiplied by the local vulnerability, which gives the local risk (Eq. 5) (Zezere et al. 2008; Remondo et al. 2008; Dewan, 2013).

$$Risk = Hazard \times Vulnerability \qquad (5)$$

The obtained landslide risk map is a quantitative and probability map (Hervas & Bobrowsky, 2009 and Corominas et al., 2014).

Therefore, the purpose of this study is to model landslide risk in Golestan Province. Risk encodes the information on both hazard and vulnerability. Hazard is more related to environmental factors (slope, aspect, elevation, etc.), while vulnerability is related to socio-economic factors, such as building density and population density. A region may have high landslide hazard while being not socio-economically vulnerable, or vice versa. Therefore, both vulnerability and hazard should be considered together for risk analysis. Therefore, the machine learning tools and environmental factors are used to prepare the landslide hazard map, but socio-economic factors and the decision-making method (FAHP) were applied to prepare a vulnerability map. Finally, our analysis leads to a hazard and vulnerability map, as discussed next. After predicting the Hazard map and preparing the Vulnerability map, the Risk map is calculated through the raster calculator tools in the ArcGIS environment based on Eq. (5)

3.4 Model performance evaluation

In this study three metrics, comprising: threshold-independent area under curve (AUC) of the receiver–operator characteristic curve (ROC), True Skill Statistic (TSS), and Accuracy (or efficiency), were used to evaluate the performance of landslide hazard models (Pontius & Schneider, 2001; Lee and Park, 2013; Shabani et al.2018; Rahmati et al. 2019; Dodangeh et al. 2020). These metrics have been broadly applied for the evaluation of machine learning models (Allouche et al., 2006; Wang, 2007; Rahmati et al. 2019).

Accuracy shows how well a test accurately identifies or excludes a condition and it is obtained by Eq. (6), where, FP is false positive, FN is false negative, TP is true positive, and TN is true negative. TP and TN are the number of pixels that are accurately classified while FP and FN are the numbers of pixels incorrectly classified (Beguería, 2006; Manfreda et al., 2014; Bui et al., 2016).

The True Skill Statistic (TSS) was calculated by Eq. (7) based on the sum of sensitivity (Eq. 8) and specificity minus 1 (Eq. 9). (Allouche et al., 2006 Shabani et al.2018; Dodangeh et al. 2020). TSS value varies from −1 to +1, where -1 demonstrates predictive capabilities of not better than a random model, 0 demonstrates an indiscriminate model and +1 a perfect model (Allouche et al., 2006).

The area under the receiver–operator characteristic curve (AUROC) provides a measure of model accuracy in predicting landslide occurrence (Gorsevski, 2006). The range of possible AUC values lies in the interval [0, 1], where values of AUC close to 1 indicate high model performance (Yesilnacar, 2005; Pearce & Ferrier, 2000; Fielding & Bell, 1997; Philips, 2004; Wang, 2007; Frattini et al. 2010).

$$Accuracy = \frac{TP + TN}{TP + TN + FP + FN} \qquad (6)$$

$$TSS = Sensitivity + Specificity - 1 \qquad (7)$$

$$Sensitivity = \frac{TP}{TP + FN} \qquad (8)$$

$$1 - Specificity = \frac{FP}{TN + FP} \qquad (9)$$

4 Results

4.1 Landslide hazard map

Figure. 6 shows the landslide hazard maps obtained with the algorithms discussed in Section 3.1, i.e, MaxEnt, SVM and GARP, by classifying hazard levels as low, moderate, high and very high. Moreover, Figure. 7 displays the results from AUC ROC statistics (see Section 3.4) on the accuracy of the different algorithms. As can be seen from Fig. 7 and table 3, the MaxEnt model delivered the best performance (AUC = 92%, TSS=82.3%, Accuracy=87.5%), followed by SVM (AUC = 81%, TSS=73.6%, Accuracy=78.3%) and GARP (AUC = 74%, TSS=66.8%, Accuracy=71.6%). Therefore, the results of MaxEnt were used to prepare landslide risk.

Table 3. Predictive performance of models using three evaluation statistics

Statistics	MaxEnt	SVM	GARP
AUCROC (%)	92	81	74
Accuracy (%)	87.5	78.3	71.6
TSS (%)	82.3	73.6	66.8

It is interesting to note that previous work also revealed slightly superior performance of MaxEnt for different applications, compared to other models (Phillips et al., 2006; Hong et al., 2016; Park, 2015; Kornejady et al., 2017). Various reasons for this behavior have been suggested, in particular the fact that MaxEnt incorporates an explicit regularization mechanism to avoid overfitting while modeling the spatial distribution of event occurrence directly, without relying on assumption of absence locations (Phillips and Dudík, 2008). However, as can be seen from the hazard maps in Fig. 6, despite the differences in model accuracy, all 3 algorithms (MaxEnt, SVM and GARP) associate the mountainous east, south and southwest areas of Golestan Province with the highest levels of landslide probability. This result is interesting, considering that these areas are characterized by complex topography, steep slopes and relatively high rainfall, and given the potential impact of local human interferences in the area (see Section 5.1).

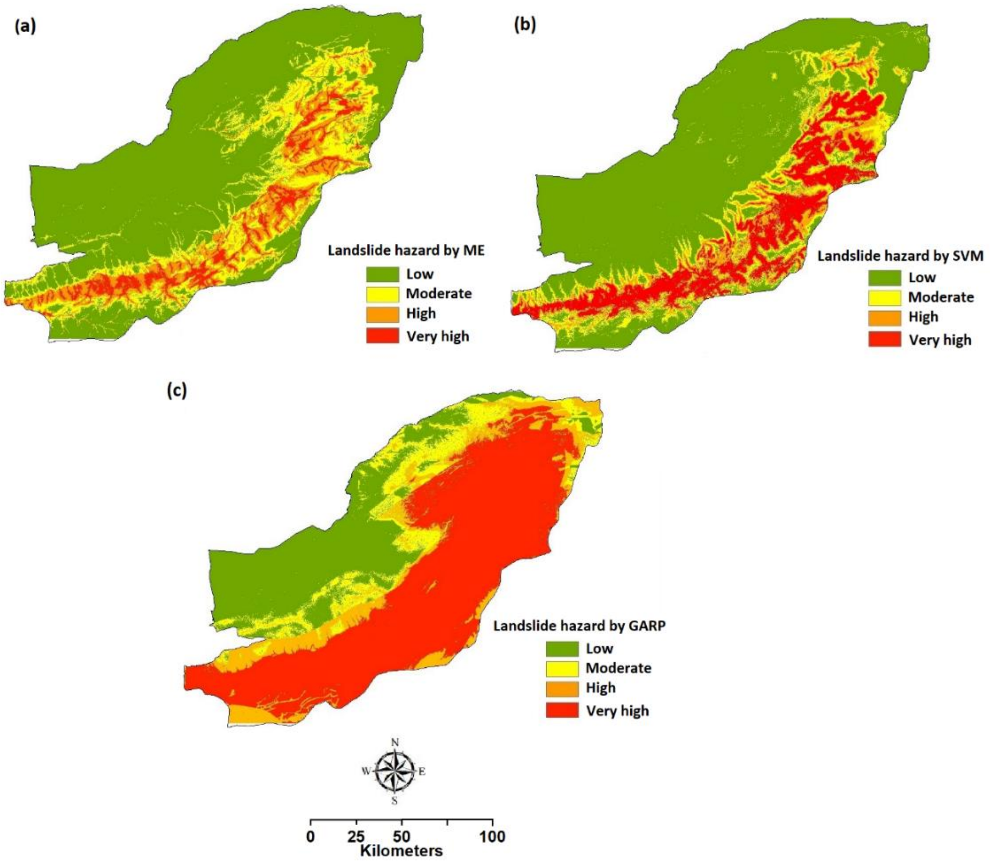

Fig. 6. Landslide hazard maps obtained for Golestan Province with the different machine learning algorithms considered in the present study: (a) Maximum Entropy (MaxEnt), (b) Support Vector Machine (SVM) and Genetic Algorithm for Rule Set Production (GARP).

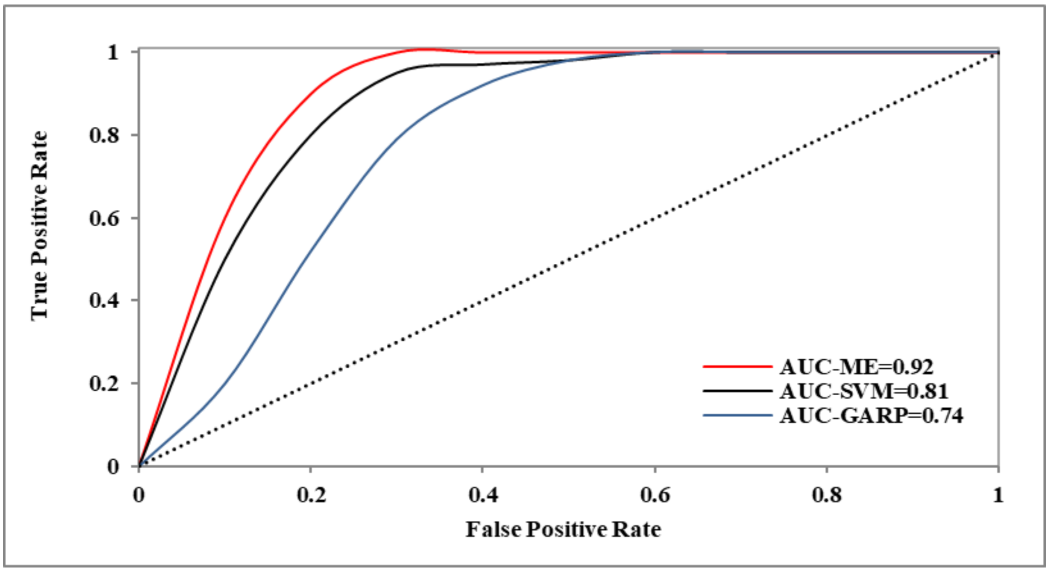

Fig. 7. Receiver operating characteristic (ROC) curves of MaxEnt, SVM and GARP algorithms in the landslide hazard mapping for Golestan Province.

4.2 Landslide vulnerability map

The results showed that the factor urban population density is the most significant vulnerability factor for Golestan Province, followed by urban building density and distance to landslide location. The normalized weights of the different factors in the framework of FAHP are shown in Fig. 8. Moreover, the consistency of the comparison matrix associated with these weights is assessed by a FAHP index called consistency ratio (CR). The smallest the value of CR, the higher the consistency of the comparison matrix (Leung and Cao, 2000). As can be seen in Fig. 8, the value of CR obtained here is significantly smaller than 10%, thus indicating acceptable consistency of the decision-making process applied.

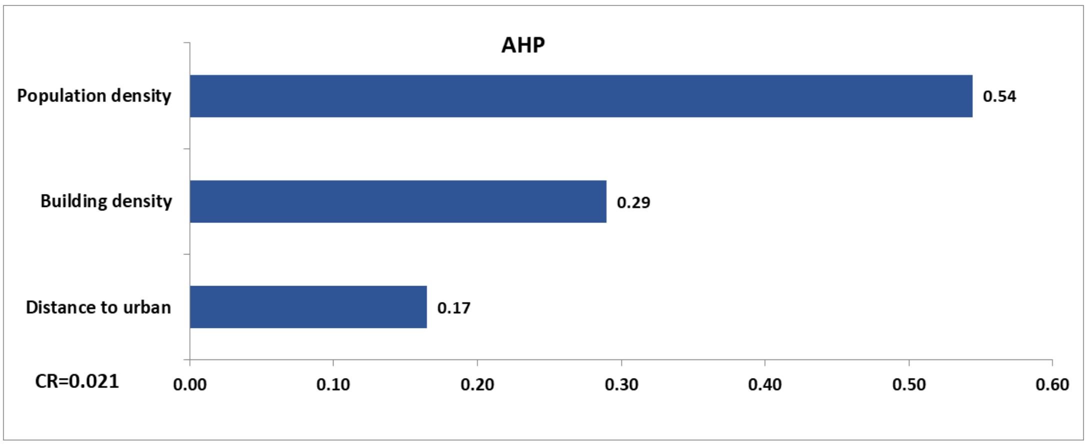

Fig. 8. Normalized weights of the vulnerability factors obtained in the framework of the FAHP computations.

Based on the results of Fig. 8 and the spatial distributions of the vulnerability factors (Fig. 5), the landslide vulnerability map was obtained. Finally, this map was categorized into four classes (Fig. 9), i.e., low, moderate, high, and very high vulnerability, which encompass 25.43%, 49.56%, 15.93%, 9.07% of the study area, respectively. According to Fig. 9, the areas of highest landslide vulnerability are located in the south and southwest of Golestan Province.

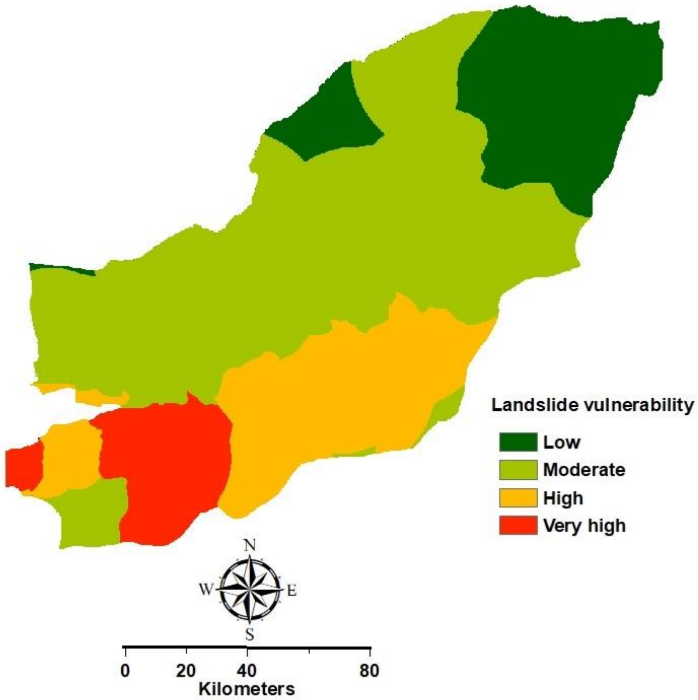

Fig. 9. Landslide vulnerability map obtained with FAHP for Golestan Province.

4.3 Landslide risk map

The landslide risk probability map (Fig. 10a) obtained from the product of the vulnerability and hazard maps and then was classified into four classes: low, moderate, high, very-high risk, corresponding to 72.47%, 17.37%, 7.85%, and 2.29% of the study area, respectively (Fig. 10b). According to this figure, the regions of highest landslide risk are the south and southwest regions of Golestan Province. We remark that our results are based on the landslide risk probability map (between 0 and 1), i.e., a quantitative map. Subsequently, we applied a classification to the results of this quantitative map to produce a new qualitative map. The landslide risk probability map is shown in Fig 10a. We further note that the output of GARP model had the highest correlation with soil map compared to other two models. Based on GARP model, the most hazardous areas in terms of landslide were located in all soil types except aridisols. Therefore, the output of GARP model is more accordance with soil map. Moreover, the MaxEnt model had the best performance and therefore the results of ME were used to prepare landslide risk (risk=hazard *vulnerability). The respective roles of the various environmental factors are discussed in the next section in the light of our results.

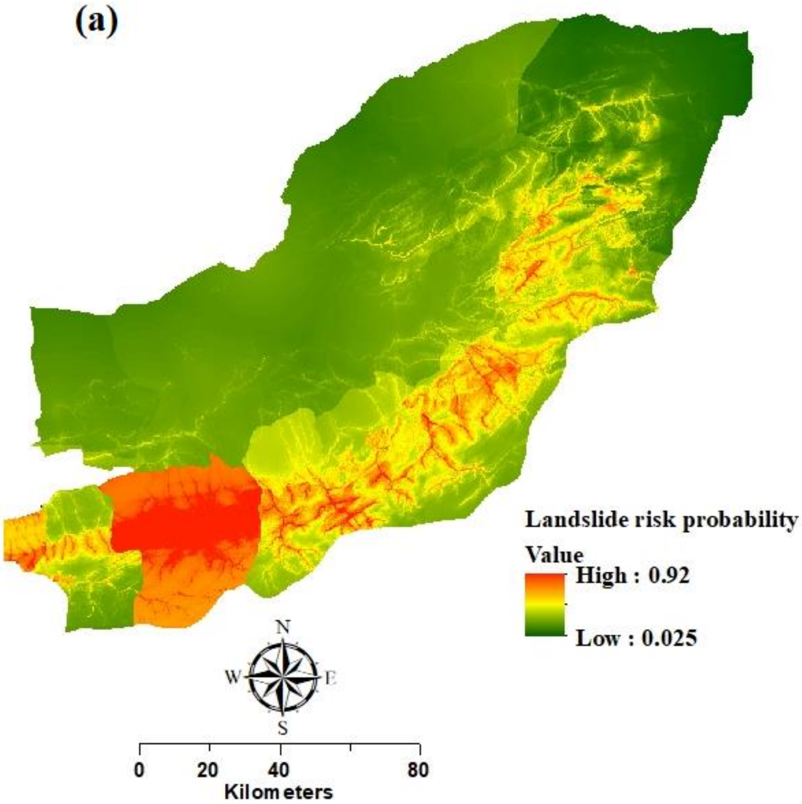

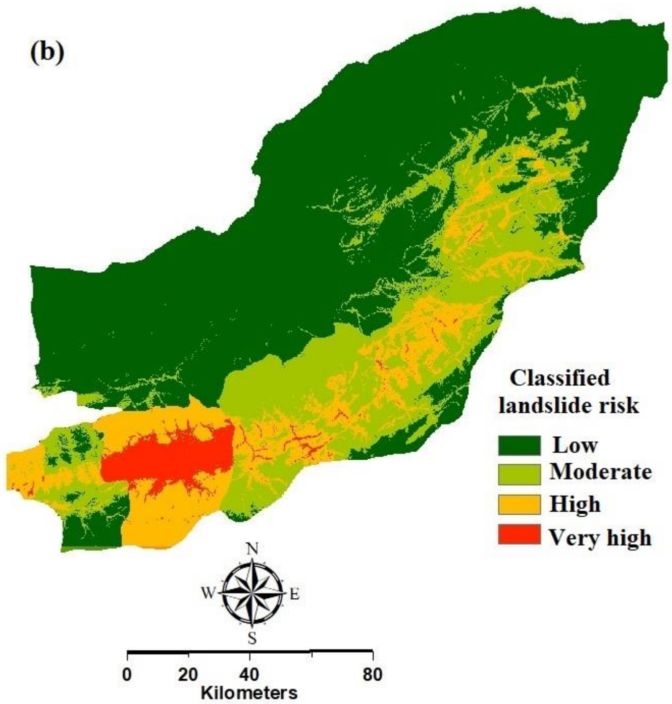

Fig. 10. Predicted landslide risk map of Golestan Province.

5 Discussion

The goal of this study is to construct a landslide risk map for Golestan Province, which can be used by the local government to identify the regions of highest landslide risk. Since a region may have high landslide hazard but little vulnerability to landslide damage (and vice-versa), the risk map produced here incorporates both hazard and vulnerability maps (Schneiderbauer & Ehrlich, 2004; Dewan, 2013; Zezere et al. 2008; Remondo et al. 2008). In the following paragraphs Fig. 10 was analyzed by discussing the role of the various human-environmental factors on landslide hazard and vulnerability in Golestan Province.

5.1 Relative influences of the landslide hazard factors in Golestan Province

To shed light into the relative influences of the different hazard factors, it can be referred to the Jackknife test results from the MaxEnt model, which are displayed in Fig. 11. In the framework of this test, the model is run with only one hazard factor at a time (under exclusion of all other factors), thus leading to the ROC AUC values denoted by the blue bars in Fig. 11. Moreover, the green bars in Fig. 11 correspond to the ROC AUC values from the complementary model, i.e., in which one of the factors at a time has been excluded from the model.

According to Fig. 11, MaxEnt identified the factors elevation, precipitation, soil type, lithology, land use/land cover and distance to river as the most relevant ones for landslide hazard in Golestan Province – all these factors have been associated with AUC > 0.7, close to the total AUC = 0.89 (red bar in Fig. 11). Moreover, according to Fig. 11, the factor slope-aspect is closest to the worst possible AUC (0.52) and has, thus, the lowest relevance, while the factors slope-angle, distance to road and distance to fault have comparable, intermediate impact on landslide hazard in the study area.

Furthermore, to better understand the functional dependence of landslide hazard on the conditional variables, it can be referred to the respective response curves displayed in Fig. 12. Each subplot in Fig. 12 shows the variations in the logistic prediction of landslide hazard as a function of the selected variable, under the constraint that the values of all other factors are considered constant and equal to their average. The response curves are briefly discussed in the next subsections.

5.1.1 Elevation

As shown in Fig. 12a, the response of landslide modeling to elevation displays two regimes, which are separated by an intermediate range of relatively constant susceptibility between 200 m and 1000 m. In regime I ($H \lesssim 200$ m), predicted landslide occurrence probability p increases with elevation H, but in regime II ($H \gtrsim 1000$ m), a negative correlation is observed.

We propose that decreased human presence and interferences at high altitudes contribute to the behavior observed in Fig. 12a. In particular, the sparse vegetation cover and the concatenated changes in land use/ land cover practice may contribute to reducing landslide probability at high altitudes. Furthermore, the lower infiltration rates associated with high elevation levels are associated with lower soil saturation (Salarian et al. 2014), thus contributing to decreasing landslide hazard. Moreover, snow precipitation may provide one further slope stabilizing agent at high elevations, although this process is still poorly understood.

We find that a logarithmic function, i.e.,

$$p = \frac{a}{H} \cdot \exp\left\{-\frac{1}{2} \cdot \left[\frac{\ln(H) - b}{c}\right]^2\right\}, \quad (10)$$

describes reasonably well the response curve of landslide occurrence probability p as a function of elevation H Golestan Province (see Fig. 13a). The best fit to the data using Eq. (10), with H in km, yields $a \approx 0.58$ km, $b \approx 0.18$ and $c \approx 0.83$, with correlation coefficient $R^2 \approx 0.96$. We note that this logarithmic function describes well the rapid increase of the susceptibility p with elevation in regime I, and the much slower decrease in regime II. Moreover, the value of $a \approx 0.58$ km is well within the intermediate range ($200 \lesssim x \lesssim 1000$) separating both regimes as estimated above. Future research is thus necessary to shed light on the values of a, b and c as a function of regional conditions.

5.1.2 Precipitation

Figure. 12b shows that landslide probability increases with increasing precipitation up to 850 mm, which suggests prevailing influence of streamflow-induced, downhill sediment transport processes in this regime. However, according to Fig. 12b that landslide probability decreases for precipitation levels higher than 850 mm. We interpret this behavior as result of increased saturation associated with such high precipitation levels, thus enhancing resistance of local lithology to water erosion and increasing soil stability in the corresponding areas.

5.1.3 Slope

Moreover, our results indicate the existence of an optimal slope of about 25° for landslide occurrence (Fig. 12c). Under high enough levels of gravitational stresses, the soil surface relaxes through landslides in the direction of steepest descent (Neuhauser & Terhorst, 2007; Dymond et al. 2006). As shown in Fig. 12c, this behavior dictates landslide probability trend in the regime of small slopes below the threshold of approximately 25° (denoted here regime I). However, the opposite trend is observed for larger slopes (regime II). We find that the dependence of response curve on slope-angle can be approximately described by the following equation:

$$p = p_0 - K \cdot (\theta - \theta_0)^2, \qquad (11)$$

where p denotes the predicted probability of landslide occurrence, θ is the slope-angle in degrees, p_0 is the value of p at $\theta = \theta_0$, which separates regimes I and II above, and K is constant that has units of degrees^{-2}. The best fit to the data using Eq. (10) gives $p_0 \approx 0.64$, $\theta_0 \approx 25.6°$ and $|K| \approx 6.6 \times 10^{-4}$, with correlation coefficient $R^2 \approx 0.96$ (see Fig. 13b).

It is interesting to note that Demir et al. (2013) also found a peak in the landslide hazard for a slope-angle θ_0 of approximately 25° at North Anatolian Fault Zone at Kelkit Valley, Turkey. As discussed by Abedini et al. (2014), geological formations on higher slopes are often associated with harder materials, which are less permeable and more resistant to gravitational stresses. Moreover, we note that, since various types of loose sediment have angle of repose in range 20° – 35°, terrain slopes exceeding this range provide rather unfavorable conditions for long-term deposition of deep granular layers, thus potentially contributing to decreasing levels of gravitational stress accumulation and landslide probability on slopes much steeper than 25°.

5.1.4 Aspect

The relationship between the slope-aspect and predicted landslide occurrence probability is shown in Fig. 12d. As can be seen from this figure, landslide hazard is highest in the north aspect (350°), which can be understood by increased heat absorption and higher humidity levels associated with this aspect (Fig. 12d). Enhanced landslide hazard for slopes facing north and northeast was also found by Demir et al (2013) in the North Anatolian Fault Zone at Kelkit Valley, Turkey. Indeed, soil response to atmospheric events depends on slope facing direction, which influences local precipitation, solar radiation and freeze-thaw processes and is thus an important component in the landslide hazard map (Demir et al. 2013). However, our results indicate that aspect has the smallest influence on landslide hazard in Golestan Province (see Fig. 11).

5.1.5 Lithology

As shown in Fig. 12e, the lowest values of landslide hazard as a function of lithology are associated with Qm (swamp and marsh) and Qsw (swamp) types, i.e., wetlands corresponding to saturated areas and relatively stable soil conditions with respect to landslide. Moreover, our results are consistent with previous observations that DCkh (limestone, locally including gypsum) and TRJs (dark grey shale and sandstone) formations are more prone to landslide occurrence (Ohlmacher, 2000), which is reflected in the high values of landslide hazard obtained from the model (Fig 12e).

5.1.6 Land use/Land cover

The results from the MaxEnt Jackknife test (Fig. 11) suggest land use/land cover as the main anthropogenic factor for landslide hazard in Golestan Province. Moreover, Fig. 12f shows that orchard and forest are the types of land with highest influence on landslide hazard. We expect orchard to substantially affect soil conditions and stability through multiple human interferences, such as irrigation. Furthermore, from Fig. 4e and Fig. 6, we see that forest areas occur within the regions associated with the highest landslide hazard levels. Indeed, forest areas are associated with high infiltration levels and have been largely affected by unprincipled road construction, which further contributes to increasing soil instability (Reichenbach et al. 2014; Leventhal & Kotze, 2008). Figure. 12f shows that land use/land cover types agriculture, urban and rangeland lead to similar values of landslide probability, which are nearly twice as large as on rock areas. These results clearly indicate the substantial effect of land use/land cover on landslide hazard and provide a basis for future considerations on land use/land cover practices in Golestan Province with regard to landslide control and mitigation.

5.1.7 Soil type

As expected, Fig. 12g shows that aridisols, consisting of stony clays and silts of slow formation rates and low degree of erodibility, lead to the lowest values of landslide hazard. By contrast, alfisols, mollisols and inceptisols are associated with higher landslide hazard (Fig. 12g), owing to their fine texture and high permeability levels, and given their suitability for land use/land cover.

5.1.8 Distance to the fault, distance to the river, distance to the road

As can be seen from Figs. 12h, 12i and 12j, landslide hazard tends to be consistently smaller the larger the distance to the next fault, river or road. Indeed, it is well known that the amplitude of a given seismic event decreases non-linearly with distance from the origin – this behavior is reflected by the dependence of landslide modeling on distance to fault in Golestan Province (Fig. 12h). Zhuang et al. (2010) found that the occurrence rate of earthquake-triggered landslides in Beichuan County, China, decreases exponentially with distance to fault. From the data of Fig. 12h, we find that the exponential decay describes approximately the response curve of landslide modeling with distance to fault, as shown in Fig. 13c. Moreover, this figure further shows that the exponential law adjusts reasonably well predicted hazard as a function of distance to river and distance to road. Specifically, the equation used to fit the data in Fig. 13c reads,

$$p = \exp(-\lambda x), \qquad (12)$$

where $1/\lambda$ denotes a characteristic length that dictates how fast the hazard decreases with distance x from the road, river or fault. The best fits to the data in Fig. 13c using Eq. (12) yield $\lambda_{\text{road}} \approx 0.0797$ km^{-1} for road ($R^2 \approx 0.83$), $\lambda_{\text{fault}} \approx 0.108$ km^{-1} for fault ($R^2 \approx 0.94$) and $\lambda_{\text{river}} \approx 0.734$ km^{-1} for river ($R^2 \approx 0.95$). The characteristic decay lengths read, thus, $1/\lambda_{\text{road}} \approx 12.5$ km, $1/\lambda_{\text{fault}} \approx 9.3$ km and $1/\lambda_{\text{river}} \approx 1.4$ km, respectively. Therefore, our results suggest that landslide hazard decreases the slowest with distance to the next road, compared to distance to the next river or fault.

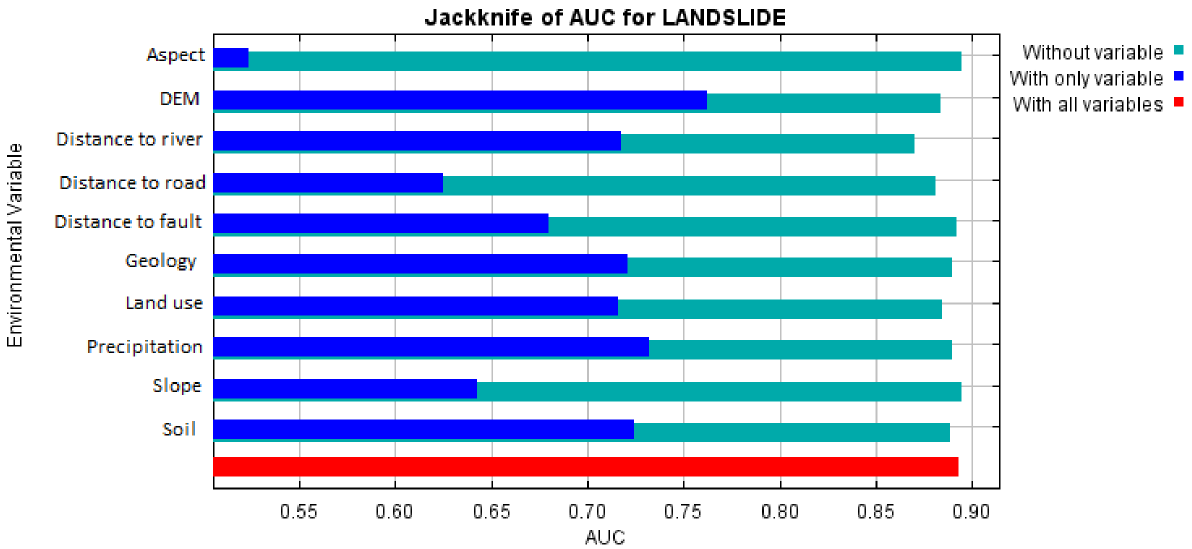

Fig. 11. Results of Jackknife test to estimate the relative influence of the various hazard factors in MaxEnt. Blue bars denote the AUC-ROC obtained with only one factor at a time (under exclusion of all other factors), the green bars give the complementary information and the red bars indicate the total AUC-ROC for MaxEnt.

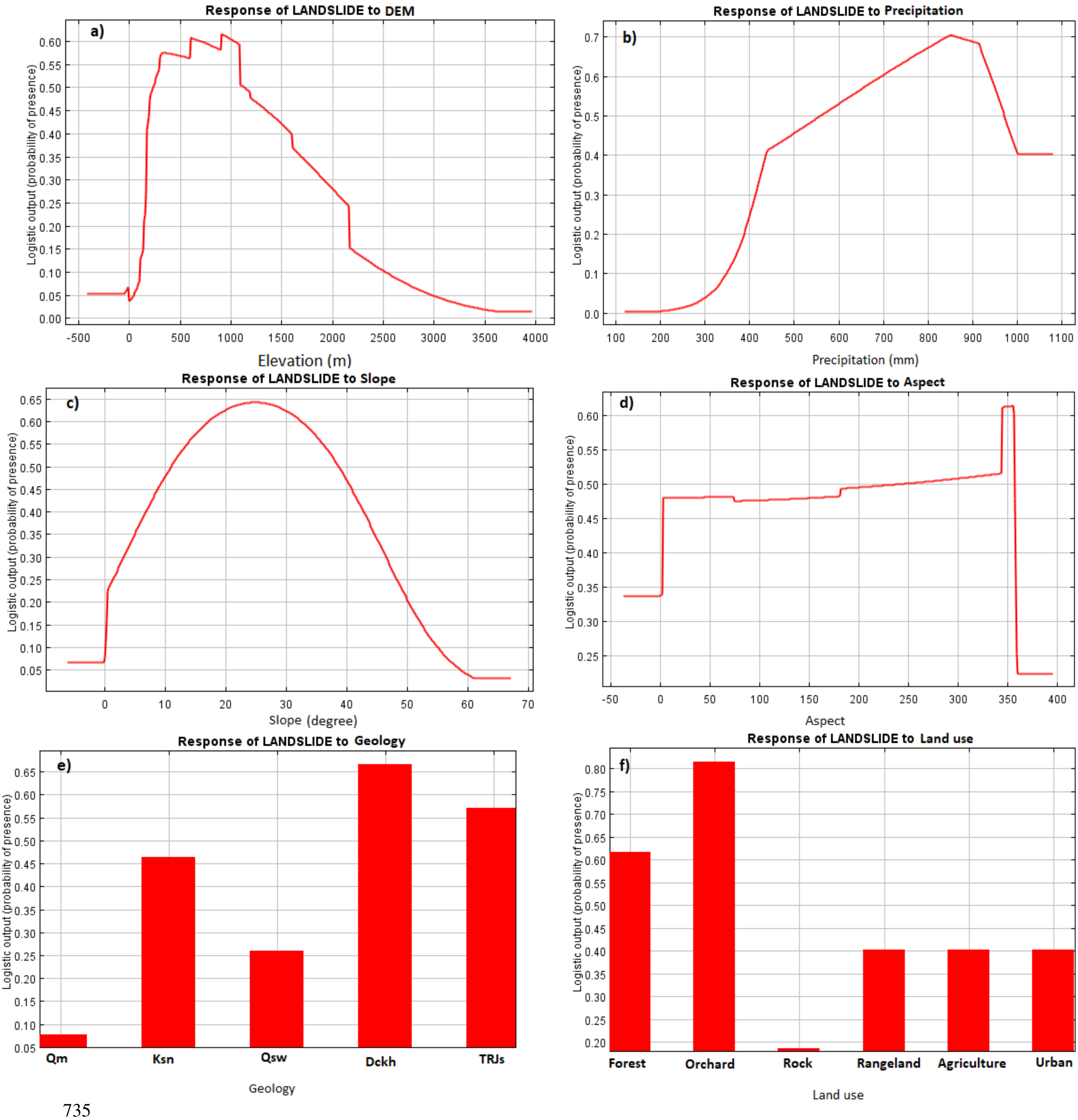

Fig. 12. Response curves of landslide modeling to the conditioning variables as predicted with MaxEnt

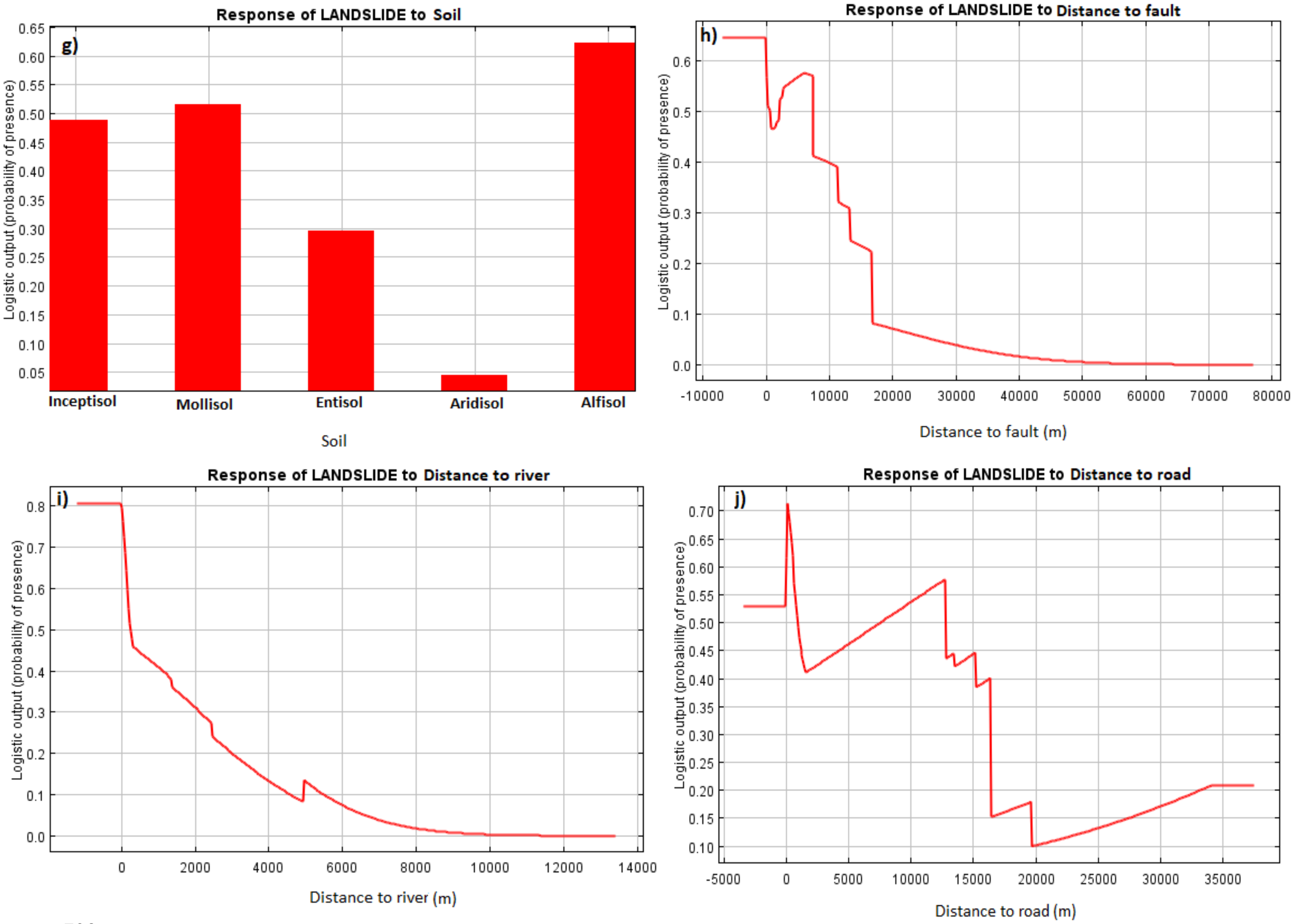

Fig. 12. continued

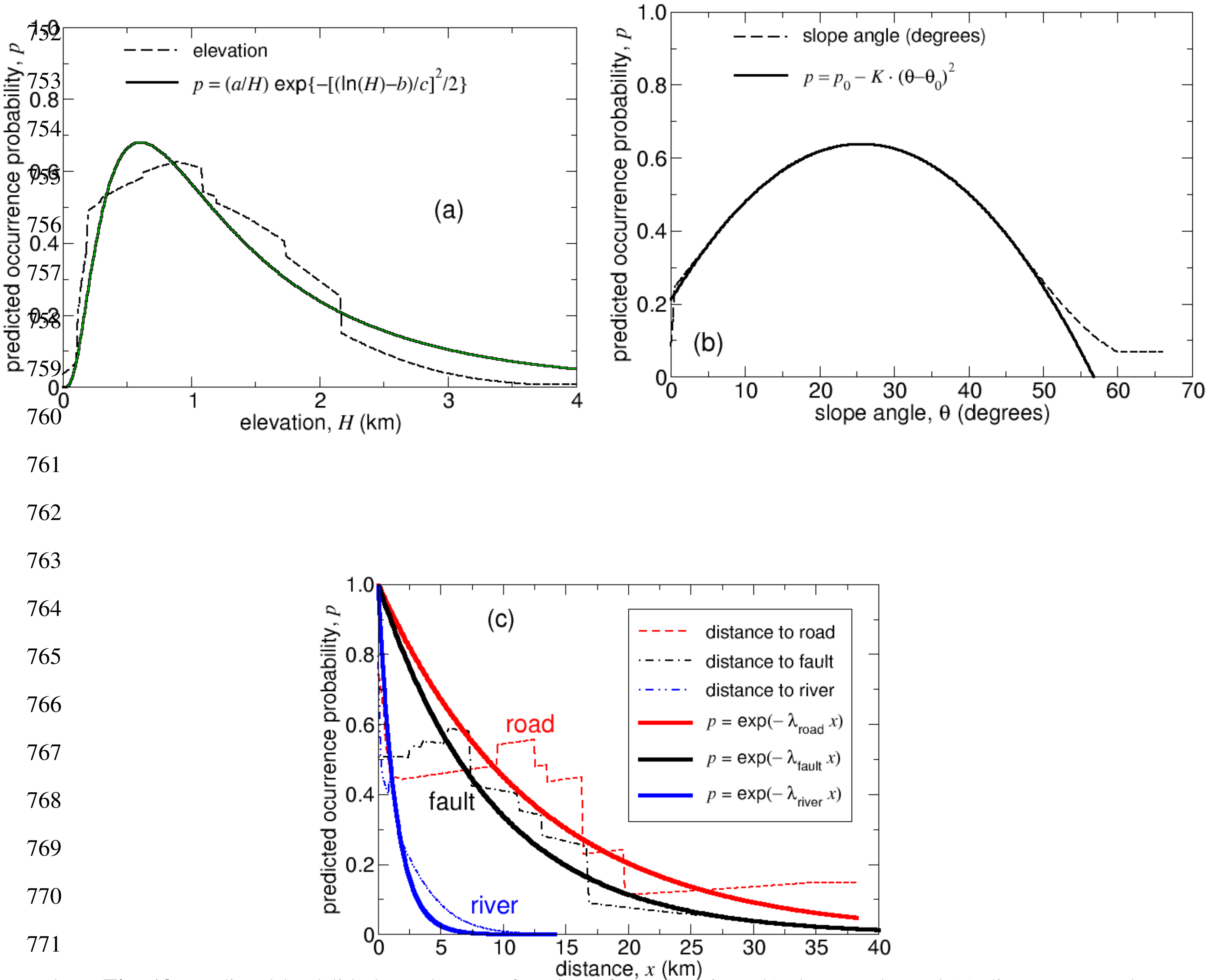

Fig. 13. Predicted landslide hazard p as a function of (a) elevation, (b) slope-angle, and (c) distance to roads, faults and rivers. Dashed and dotted lines denote data from the hazard map, while continuous lines denote best fits using Eqs. (10), (11) and (12) for subplots (a), (b) and (c), respectively. The values of the parameters obtained from these fits read: (a) $a \approx 0.58$ km, $b \approx 0.18$ and $c \approx 0.83$ ($R^2 \approx 0.96$); (b) $\theta_0 \approx 25.6°$, $p_0 \approx 0.64$ and $|K| \approx 6.6 \times 10^{-4}$ ($R^2 \approx 0.96$), and (c) $\lambda_{\text{road}} \approx 0.0797$ km^{-1} ($R^2 \approx 0.83$), $\lambda_{\text{fault}} \approx 0.108$ km^{-1} ($R^2 \approx 0.94$) and $\lambda_{\text{river}} \approx 0.734$ km^{-1} ($R^2 \approx 0.95$).

5.2 Vulnerability and risk: implications for landslide control and mitigation strategies

The results discussed in the previous section yield new insights about landslide hazard as a function of the anthropogenic and environmental conditioning variables. For instance, from the considerations above, recommendations can be derived for road construction with regard of the distance to populated areas, while optimization strategies for land use/land cover changes can be developed to decreasing the impact of anthropogenic influences on landslide initiation.

However, because risk encodes both landslide probability and the associated level of damage, knowledge of the spatial distribution of vulnerability is required to improving risk management. By combining the hazard map (Fig. 6) with the vulnerability map (Fig. 9), as described in Section 3.3, it is found that the south and southwest areas of Golestan Province are associated with the highest landslide risk levels. These regions encompass Gorgan city, the center of Golestan Province, and have, correspondingly, particularly high urban population and building density. Risk in Golestan Province has been assessed high throughout the entire region of very high landslide hazard, i.e., from southwest to the east (compare Figs. 6 and 10), but the area of highest risk level is located in the southwest – the location of Gorgan city. The risk level distribution in Fig. 10 provides governmental agencies and stakeholders, thus, with more appropriate information to guide priority plans for landslide mitigation in Golestan Province.

5.3 Final remarks and outlook

Summarizing, risk is function of vulnerability and hazard. Vulnerability is related to socio-economic factors, while hazard is related to environmental factors. In previous work (Mokhtari et al. 2020), risk was modeled by considering hazard only, thereby incorporating environmental factors, but ignoring vulnerability factors. By contrast, here we considered *both* vulnerability *and* hazard to compute the landslide risk map for Golestan Province. Firstly, we obtained the landslide hazard map based on the environmental factors (slope, elevation, etc.) and landslide occurrence observation points. Subsequently, we calculated the landslide vulnerability map based on socio-economic factors (population density, etc.), and obtained the landslide risk map from the combination of *both* landslide hazard *and* landslide vulnerability maps.

It should be noted that including landslide size and duration in our statistics would greatly improve the assessment of landslide distribution. However, unfortunately, in the study area considered in our work, the statistics of the extent of sliding and the time of the occurrence of the landslides is not available. Furthermore, our goal in this manuscript is to provide an estimate of landslide occurrence distribution without regard of the time of the duration and size of the individual landslide events. Therefore, the methods employed in our work employ the information on landslide locations to produce the landslide hazard maps. We further refer to previous work in which landslide hazard has been evaluated based solely on landslide occurrence points (Pourghasemi et al., 2013; Aghdam et al., 2017; Adineh et al., 2018).

We further note that we could not monitor the whole area of Golestan Province because it was not possible to access all parts of the map. In the machine learning modeling employed, the distribution of the samples does not affect the modeling process because the geographic locations are not used as input. Rather, the similarity of characteristics in each pixel with trained pixels affects the model output. We nevertheless believe that our analysis is providing a valuable contribution as it is paving the way toward a future quantitative modeling of hazard and vulnerability in Golestan Province, and because our discussion section is including yet unreported mathematical expressions relating landslide hazard and causative factors. These mathematical expressions are physically based and grounded on the dynamics of landslide occurrence that have been discussed extensively in previous work. Therefore, it is noticeable that our statistics, which unfortunately misses the information of duration and magnitude of the individual landslides (not available for Golestan Province), allows us to develop a mathematical model based on the machine learning computations and the observation map. We believe that this first step will motivate future modelers to go beyond the mere computation of a risk map, i.e., that future modelers will follow our work to elaborating mathematical expressions thus increasing both the predictive power and the physical understanding of their Machine Learning results – however by including event duration and magnitude.

6 Conclusion

In conclusion, the landslide risk map was computed for Golestan Province, Iran, from an explicit consideration of all main relevant local human-environmental landslide hazard and vulnerability factors. To this end, the spatial distributions of landslide location occurrences and conditioning variables have been combined using machine learning algorithms – specifically, GARP, SVM and MaxEnt – to obtain a regional landslide hazard model for Golestan Province. This model was then coupled with the information of local landslide vulnerability, by taking the local urban population and building densities, as well as the distance to landslide locations into account.

Moreover, to generate the landslide vulnerability map, the Fuzzy Analytical Hierarchical Process (FAHP) method was applied. FAHP has been developed for multi-criteria decision-making problems involving many variables and has proven here potentially useful to improving priority landslide control plans.

Based on our results, empirical expressions were obtained for predicting landslide occurrence probability as a function of elevation, slope-angle, and distance to roads, faults and rivers. It would be interesting to verify the applicability of these equations to other regional settings, based on observations of landslide hazard, to shed light on the physical mechanisms underlying the values of the parameters associated.

Our results show that, to accurately assessing landslide risk, event occurrence probability must be considered against the background of its potential damage level. Although a strongly landslide-prone region extending from southwest to east of Golestan Province is clearly visible in the hazard map, a subset of this area, which surrounds Gorgan City, is associated with the highest landslide risk level in the risk map. This result is explained by integration of the vulnerability map into the hazard evaluation. More precisely, Gorgan City represents the area of highest urban population density *and* is located within the regions associated with very high hazard. Moreover, we have found that landslide hazard decreases approximately exponentially with distance to faults, roads and rivers, and that there is an optimal slope for landslide hazard.

We emphasize that the computation of risk performed here relies on knowledge about the distribution of the main conditioning variables, and that changes in the specific choice and relative weights of the vulnerability factors may lead to slight differences in the final risk map. Therefore, these weights must be estimated a priori, from reliable and comprehensive data on local socio-economic and environmental conditions. As shown here, FAHP indicated consistent estimates of the different vulnerability factor weights. Moreover, we have found similar results for landside hazard distribution without regard of the machine learning method considered – notwithstanding the observed differences in model accuracy – thus allowing us to discuss on the functional relationship between hazard and the different conditioning variables. Our findings provide insights for the assessment of landslide hazard, anthropogenic influences and risk, and are relevant to local governmental agencies and stakeholders with regard to optimizing regional landslide control, mitigation and management.

Acknowledgments

The authors wish to thank the Geological Survey and Mineral Explorations of Iran (GSI) for preparing maps, data and reports. EJRP thanks the German Research Foundation for funding through the Heisenberg Programme (project number 434377576).

Compliance with ethical standards

Conflicts of interest Authors declare they have no conflict of interest

References

Abay, A., Barbieri, G., & Woldearegay, K. (2019). GIS-based Landslide Susceptibility Evaluation Using Analytical Hierarchy Process (AHP) Approach: The Case of Tarmaber District, Ethiopia. Momona Ethiopian Journal of Science, 11(1): 14-36.

Abdulwahid, W. M., & Pradhan, B. (2017). Landslide vulnerability and risk assessment for multi-hazard scenarios using airborne laser scanning data (LiDAR). Landslides, 14(3): 1057-1076.

Abedini, M., Ghasemian, B. & Shirzadi, A. (2014). Modeling landslide hazard using statistical model of logistic regression (case study: Kurdistan province, Bijar city). Geography and Development 37: 85-102. (In Persian)

Achour, Y. & Pourghasemi, H. R. (2020). How do machine learning techniques help in increasing accuracy of landslide susceptibility maps? Geoscientific Frontiers 11(3): 871-883.

Adineh, F., Motamedvaziri, B., Ahmadi, H., & Moeini, A. (2018). Landslide susceptibility mapping using Genetic Algorithm for the Rule Set Production (GARP) model. Journal of Mountain Science, 15(9): 2013-2026.

Alkhasawneh, M. S., Ngah, U. K., Tay, L. T., & Isa, N. A. M. (2014). Determination of importance for comprehensive topographic factors on landslide hazard mapping using artificial neural network. Environmental earth sciences, 72(3): 787-799.

Allen, M. B., Ghassemi, M. R., Shahrabi, M., & Qorashi, M. (2003). Accommodation of late Cenozoic oblique shortening in the Alborz range, northern Iran. Journal of structural geology, 25(5): 659-672.

Alonso, J. A. & Lamata, M. T. (2006). Consistency in the analytic hierarchy process: a new approach. International Journal of Uncertainty, Fuzziness and Knowledge-Based Systems, 14(4): 445-459.

Althuwaynee, O. F., Pradhan, B., & Ahmad, N. (2015). Estimation of rainfall threshold and its use in landslide hazard mapping of Kuala Lumpur metropolitan and surrounding areas. Landslides, 12(5): 861-875.

Armaş, I. (2011). An analytic multicriteria hierarchical approach to assess landslide vulnerability. Case study: Cornu village, Subcarpathian Prahova Valley/Romania. Zeitschrift für Geomorphologie, 55(2): 209-229.

Ashournejad, Q., Hosseini, A., Pradhan, B., & Hosseini, S. J. (2019). Hazard zoning for spatial planning using GIS-based landslide susceptibility assessment: a new hybrid integrated data-driven and knowledge-based model. Arabian Journal of Geosciences, 12(4): 126.

Axen, G. J., Lam, P. S., Grove, M., Stockli, D. F., & Hassanzadeh, J. (2001). Exhumation of the west-central Alborz Mountains, Iran, Caspian subsidence, and collision-related tectonics. Geology, 29(6): 559-562.

Azareh, A., Rahmati, O., Rafiei-Sardooi, E., Sankey, J. B., Lee, S., Shahabi, H., & Ahmad, B. B. (2019). Modelling gully-erosion susceptibility in a semi-arid region, Iran: Investigation of applicability of certainty factor and maximum entropy models. Science of the Total Environment, 655: 684-696.

Ballabio, C., & Sterlacchini, S. (2012). Support vector machines for landslide susceptibility mapping: the Staffora River Basin case study, Italy. Mathematical geosciences, 44(1): 47-70.

Beakawi Al-Hashemi, H. M. & Baghabra Al-Amoudi, O. (2018). A review on the angle of repose of granular materials. Powder Technology. 330: 397-417.

Bhushan, N., & Rai, K. (2007). Strategic decision making: applying the analytic hierarchy process. Springer Science & Business Media.1-171.

Boeckmann, M., & Joyner, T. A. (2014). Old health risks in new places? An ecological niche model for I. ricinus tick distribution in Europe under a changing climate. Health & Place, 30: 70-77.

Brabb, E. E. (1985). Innovative approaches to landslide hazard and risk mapping. In International Landslide Symposium Proceedings, Toronto, Canada.1: 17-22.

Brenning, A., Schwinn, M., Ruiz-Páez, A. P. & Muenchow, J. (2015). Landslide susceptibility near highways is increased by 1 order of magnitude in the Andes of southern Ecuador, Loja province, Natural Hazards and Earth System Science, 15: 45–57.

Bui, D. T., Tsangaratos, P., Nguyen, V. T., Van Liem, N., & Trinh, P. T. (2020). Comparing the prediction performance of a Deep Learning Neural Network model with conventional machine learning models in landslide susceptibility assessment. *Catena*, *188*, 104426.

Carver, S. J. (1991). Integrating multi-criteria evaluation with geographical information systems. International Journal of Geographical Information System, 5(3): 321-339.

Catani, F., Lagomarsino, D., Segoni, S. & Tofani, V. (2013). Landslide susceptibility estimation by random forests technique: sensitivity and scaling issues, Natural Hazards and Earth System Sciences 13: 2815–2831.

Chacon, J., Irigaray, C., Fernandez, T. E. l., Hamdouni, R., (2006). Engineering geology maps: landslides and geographical information systems. Bulletin of Engineering Geology and the Environment 65: 341-411.

Chen, W., Li, W., Chai, H., Hou, E., Li, X., & Ding, X. (2016). GIS-based landslide susceptibility mapping using analytical hierarchy process (AHP) and certainty factor (CF) models for the Baozhong region of Baoji City, China. Environmental Earth Sciences, 75(1): 63.

Chen, W., Pourghasemi, H. R., Kornejady, A., & Zhang, N. (2017a). Landslide spatial modeling: Introducing new ensembles of ANN, MaxEnt, and SVM machine learning techniques. Geoderma, 305: 314-327.

Chen, W., Pourghasemi, H. R., Panahi, M., Kornejady, A., Wang, J., Xie, X., & Cao, S. (2017b). Spatial prediction of landslide susceptibility using an adaptive neuro-fuzzy inference system combined with frequency ratio, generalized additive model, and support vector machine techniques. Geomorphology, 297: 69-85.

Convertino, M., Troccoli, A., & Catani, F. (2013). Detecting fingerprints of landslide drivers: a MaxEnt model. Journal of Geophysical Research: Earth Surface, 118(3): 1367-1386.

Corominas J., van Westen C., Frattini P., Cascini L., Malet J. P., Fotopoulou S., Catani F., Van Den Eeckhaut M., Mavrouli O., Agliardi F., Pitilakis K., Winter M. G., Pastor M., Ferlisi S., Tofani V., Hervás J. & Smith J. T., (2014). Recommendations for the quantitative analysis of landslide risk. Bulletin of Engineering Geology and the Environment 73:209-263.

Cutter, S. L., Boruff, B. J., & Shirley, W. L. (2003). Social vulnerability to environmental hazards. Social Science Quarterly, 84(2): 242-261.

Dai, F. C., & Lee, C. F. (2002). Landslide characteristics and slope instability modeling using GIS, Lantau Island, Hong Kong. Geomorphology, 42(3-4): 213-228.

Dai, F. C., Lee, C. F., & Ngai, Y. Y. (2002). Landslide risk assessment and management: an overview. Engineering Geology, 64(1): 65-87.

Dai, F. C., Lee, C. F., Li, J. X. Z. W., & Xu, Z. W. (2001). Assessment of landslide susceptibility on the natural terrain of Lantau Island, Hong Kong. Environmental Geology, 40(3): 381-391.

Darabi, H., Choubin, B., Rahmati, O., Haghighi, A. T., Pradhan, B., & Kløve, B. (2019). Urban flood risk mapping using the GARP and QUEST models: A comparative study of machine learning techniques. Journal of Hydrology, 569: 142-154.

de Blasio, F. V. (2011). Introduction to the Physics of Landslides: Lecture Notes on the Dynamics of Mass Wasting. Springer Science & Business Media, 408 pp.

de Souza Muñoz, M. E., De Giovanni, R., de Siqueira, M. F., Sutton, T., Brewer, P., Pereira, R. S., ... & Canhos, V. P. (2011). openModeller: a generic approach to species' potential distribution modelling. GeoInformatica, 15(1): 111-135.

Demir, G., Aytekin, M., Akgün, A., Ikizler, S. B., & Tatar, O. (2013). A comparison of landslide susceptibility mapping of the eastern part of the North Anatolian Fault Zone (Turkey) by likelihood-frequency ratio and analytic hierarchy process methods. Natural Hazards, 65(3): 1481-1506.

Dewan, A. (2013). Floods in a megacity: geospatial techniques in assessing hazards, risk and vulnerability. Dordrecht: Springer. 119-156.

Dhurmea, K. R., Boojhawon, R., & Rughooputh, S. D. D. V. (2009). Geostatistical approaches for estimating rainfall over Mauritius. *3rd Research Week*, *2010*.

Duman, T. Y., Can, T., Gokceoglu, C., Nefeslioglu, H. A., & Sonmez, H. (2006). Application of logistic regression for landslide susceptibility zoning of Cekmece Area, Istanbul, Turkey. Environmental Geology, 51(2): 241-256.

Dymond, J. R., Ausseil, A. G., Shepherd, J. D., & Buettner, L. (2006). Validation of a region-wide model of landslide susceptibility in the Manawatu–Wanganui region of New Zealand. Geomorphology, 74(1-4): 70-79.

El Bcharia, F., Theilen-Willigeb, B., & Malek, H. A. (2019, July). Landslide hazard zonation assessment using GIS analysis at the coastal area of Safi (Morocco). In Proceedings of the ICA (Vol. 2).

Elith, J., Phillips, S. J., Hastie, T., Dudík, M., Chee, Y. E., & Yates, C. J. (2011). A statistical explanation of MaxEnt for ecologists. Diversity and distributions, 17(1): 43-57.

Ercanoglu, M., & Gokceoglu, C. (2002). Assessment of landslide susceptibility for a landslide-prone area (north of Yenice, NW Turkey) by fuzzy approach. Environmental Geology, 41(6): 720-730.

Ercanoglu, M., & Gokceoglu, C. (2004). Use of fuzzy relations to produce landslide susceptibility map of a landslide prone area (West Black Sea Region, Turkey). Engineering Geology, 75(3-4): 229-250.

Erener, A., & Düzgün, H. S. B. (2012). Landslide susceptibility assessment: what are the effects of mapping unit and mapping method? Environmental Earth Sciences, 66(3): 859-877.

Feizizadeh, B., Blaschke, T., Nazmfar, H., & Rezaei Moghaddam, M. H. (2013). Landslide susceptibility mapping for the Urmia Lake basin, Iran: a multi-criteria evaluation approach using GIS. International Journal of Environmental Research, 7(2): 319-336.

Feizizadeh, B., Jankowski, P., & Blaschke, T. (2014). A GIS based spatially-explicit sensitivity and uncertainty analysis approach for multi-criteria decision analysis. Computers & Geosciences, 64: 81-95.

Felicísimo, Á. M., Cuartero, A., Remondo, J., & Quirós, E. (2013). Mapping landslide susceptibility with logistic regression, multiple adaptive regression splines, classification and regression trees, and maximum entropy methods: a comparative study. Landslides, 10(2): 175-189.

Fell, R., Corominas, J., Bonnard, C., Cascini, L., Leroi, E., & Savage, W. Z. (2008). Guidelines for landslide susceptibility, hazard and risk zoning for land-use planning. Engineering Geology, 102(3-4), 99-111.

Fielding, A. H., & Bell, J. F. (1997). A review of methods for the assessment of prediction errors in conservation presence/absence models. Environmental Conservation, 24(1): 38-49.

Frigerio, I., & De Amicis, M. (2016). Mapping social vulnerability to natural hazards in Italy: A suitable tool for risk mitigation strategies. Environmental Science & Policy, 63: 187-196.

Galli, M & Guzzetti, F (2007). Landslide vulnerability criteria: A case study from Umbria, central Italy. Environmental Management, 40: 649-664.

Ghorbanzadeh, O., Blaschke, T., Gholamnia, K., Meena, S. R., Tiede, D., & Aryal, J. (2019). Evaluation of different machine learning methods and deep-learning convolutional neural networks for landslide detection. *Remote Sensing*, *11*(2): 196.

Glade, T. and Crozier, M.J., (2005a). The nature of landslide hazard impact. In: Glade, T., Anderson, M.G. and Crozier, M.J. (eds.) Landslide risk assessment. John Wiley, 43-74.

Glade, T. and Crozier, M.J., (2005b). A review of scale dependency in landslide hazard and risk analysis. In: Glade, T., Anderson, M.G. and Crozier, M.J. (eds.) Landslide hazard and risk, John Wiley, 75-138.

Glade, T., Anderson, M. G. and Crozier, M. J. (eds.), (2005c). Landslide risk assessment, John Wiley, 832 p.

Goetz, J. N., Brenning, A., Petschko, H., & Leopold, P. (2015). Evaluating machine learning and statistical prediction techniques for landslide susceptibility modeling. Computers & Geosciences, 81: 1-11.

Gorsevski, P. V., & Jankowski, P. (2010). An optimized solution of multi-criteria evaluation analysis of landslide susceptibility using fuzzy sets and Kalman filter. Computers & Geosciences, 36(8): 1005-1020.

Gorsevski, P. V., Gessler, P. E., Boll, J., Elliot, W. J., & Foltz, R. B. (2006). Spatially and temporally distributed modeling of landslide susceptibility. Geomorphology, 80(3-4): 178-198.

Guillard-Gonçalves, C., & Zêzere, J. (2018). Combining Social Vulnerability and Physical Vulnerability to Analyse Landslide Risk at the Municipal Scale. Geosciences, 8(8): 294.

Guzzetti, F., (2005), Landslide Hazard and Risk Assessment. PhD dissertation, Rheinischen Friedrich-Wilhelms-Univestitat Bonn, Germany, p. 373.

Guzzetti, F., Mondini, A. C., Cardinali, M., Fiorucci, F., Santangelo, M., Chang, k.T., (2012). Landslide inventory maps: New tools for an old problem. Earth-Science Reviews, 112:42-66.

Guzzetti, F., Mondini, A. C., Cardinali, M., Fiorucci, F., Santangelo, M., Chang, k.T., (2012). Landslide inventory maps: New tools for an old problem. Earth-Science Reviews, 112:42-66.

Hastie, T., Tibshirani, R., & Friedman, J. (2017). The Elements of Statistical Learning: Data Mining, Inference, and Prediction. Springer, New York, 745 pp.

Hervas, J., Bobrowsky, P., 2009. Mapping: Inventories, Susceptibility, Hazard and Risk: in book on Landslides - Disaster Risk Reduction, Springer-Verlag Berlin Heidelberg, ISBN: 978-3-540-69966-8, pp.

Hofmann, T., Schölkopf, B., & Smola, A. J. (2008). Kernel methods in machine learning. The Annals of Statistics, 1171-1220.

Hong, H., Naghibi, S.A., Pourghasemi, H.R. & Pradhan, B. (2016). GIS-based landslide spatial modeling in Ganzhou City, China. Arab. J. Geosci. 9 (2): 1–26.

Hong, Y., Adler, R., & Huffman, G. (2006). Evaluation of the potential of NASA multi-satellite precipitation analysis in global landslide hazard assessment. Geophysical Research Letters, 33(22).

Kalantar, B., Pradhan, B., Naghibi, S. A., Motevalli, A., & Mansor, S. (2018). Assessment of the effects of training data selection on the landslide susceptibility mapping: a comparison between support vector machine (SVM), logistic regression (LR) and artificial neural networks (ANN). Geomatics, Natural Hazards and Risk, 9(1): 49-69.

Karsli, F., Atasoy, M., Yalcin, A., Reis, S., Demir, O. & Gokceoglu, C. (2009). Effects of land-use changes on landslides in a landslide-prone area (Ardesen, Rize, NE Turkey). Environmental Monitoring and Assessment 156: 241-255.

Kawagoe, S., Kazama, S., & Sarukkalige, P. R. (2010). Probabilistic modelling of rainfall induced landslide hazard assessment. Hydrology and Earth System Sciences, 14(6): 1047-1061.

Kecman, V. (2005). Support vector machines–an introduction. In Support vector machines: theory and applications.Springer, Berlin, Heidelberg. 1-47.

Kjekstad, O., & Highland, L. (2009). Economic and social impacts of landslides. In Landslides–disaster risk reduction. Springer, Berlin, Heidelberg. 573-587.

Kornejady, A., Ownegh, M., & Bahremand, A. (2017). Landslide susceptibility assessment using maximum entropy model with two different data sampling methods. Catena, 152: 144-162.

Kumar, R., & Anbalagan, R. (2015). Landslide susceptibility zonation in part of Tehri reservoir region using frequency ratio, fuzzy logic and GIS. Journal of Earth System Science, 124(2): 431-448.

Kumar, S., & Stohlgren, T. J. (2009). Maxent modeling for predicting suitable habitat for threatened and endangered tree Canacomyrica monticola in New Caledonia. Journal of Ecology and the Natural Environment, 1(4): 094-098.

Lato, M. J., Anderson, S., & Porter, M. J. (2019). Reducing Landslide Risk Using Airborne Lidar Scanning Data. Journal of Geotechnical and Geoenvironmental Engineering, 145(9): 06019004.

Lee, S. (2007). Application and verification of fuzzy algebraic operators to landslide susceptibility mapping. Environmental Geology, 52(4): 615-623.

Lee, S., Hong, S. M., & Jung, H. S. (2017). A support vector machine for landslide susceptibility mapping in Gangwon Province, Korea. Sustainability, 9(1): 48.

Lepore, C., Kamal, S. A., Shanahan, P., & Bras, R. L. (2012). Rainfall-induced landslide susceptibility zonation of Puerto Rico. Environmental Earth Sciences, 66(6): 1667-1681.

Leung, L. C., & Cao, D. (2000). On consistency and ranking of alternatives in fuzzy AHP. *European journal of operational research*, *124*(1):102-113.

Leventhal, A. R., & Kotze, G. P. (2008). Landslide susceptibility and hazard mapping in Australia for land-use planning—with reference to challenges in metropolitan suburbia. Engineering Geology, 102(3-4): 238-250.

Malczewski, J. (1999). GIS and multicriteria decision analysis. John Wiley & Sons. 1-134.

Marjanović, M., Kovačević, M., Bajat, B., & Voženílek, V. (2011). Landslide susceptibility assessment using SVM machine learning algorithm. Engineering Geology, 123(3): 225-234.

Mehrnews (2020, May 5). Retrieved from https://www.mehrnews.com/news/4917132

Michael, E. A., & Samanta, S. (2016). Landslide vulnerability mapping (LVM) using weighted linear combination (WLC) model through remote sensing and GIS techniques. Modeling Earth Systems and Environment, 2(2): 88.

Mirzaei, G., Soltani, A., Soltani, M., & Darabi, M. (2018). An integrated data-mining and multi-criteria decision-making approach for hazard-based object ranking with a focus on landslides and floods. Environmental Earth Sciences, 77(16): 581.

Mohammady, M., Pourghasemi, H. R., & Pradhan, B. (2012). Landslide susceptibility mapping at Golestan Province, Iran: a comparison between frequency ratio, Dempster–Shafer, and weights-of-evidence models. *Journal of Asian Earth Sciences*, *61*: 221-236.

Mohan, A., Singh, A. K., Kumar, B., & Dwivedi, R. (2020). Review on remote sensing methods for landslide detection using machine and deep learning. *Transactions on Emerging Telecommunications Technologies*, e3998.

Mokhtari, M., & Abedian, S. (2019). Spatial prediction of landslide susceptibility in Taleghan basin, Iran. Stochastic Environmental Research and Risk Assessment, 33(7): 1297-1325.

Mokhtari, M., Hoseinzade, Z., & Shirani, K. (2020). A comparison study on landslide prediction through FAHP and Dempster–Shafer methods and their evaluation by P–A plots. *Environmental Earth Sciences*, *79*(3): 1-13.

Mosavi, A., Sajedi-Hosseini, F., Choubin, B., Taromideh, F., Rahi, G., & Dineva, A. A. (2020). Susceptibility mapping of soil water erosion using machine learning models. Water, 12(7): 1995.

Murillo-García, F. G., Rossi, M., Ardizzone, F., Fiorucci, F., & Alcántara-Ayala, I. (2017). Hazard and population vulnerability analysis: a step towards landslide risk assessment. Journal of Mountain Science, 14(7): 1241-1261.

Murillo-García, F., Rossi, M., Fiorucci, F., & Alcántara-Ayala, I. (2015). Population Landslide vulnerability evaluation: The case of the indigenous population of Pahuatlán-Puebla, Mexico. In Engineering Geology for Society and Territory, Springer, Cham. 2: 793-1797.

Neuhäuser, B., & Terhorst, B. (2007). Landslide susceptibility assessment using "weights-of-evidence" applied to a study area at the Jurassic escarpment (SW-Germany). Geomorphology, 86(1-2): 12-24.

Ngo, P. T. T., Panahi, M., Khosravi, K., Ghorbanzadeh, O., Kariminejad, N., Cerda, A., & Lee, S. (2021). Evaluation of deep learning algorithms for national scale landslide susceptibility mapping of Iran. *Geoscience Frontiers*, *12*(2): 505-519.

Ohlmacher, G. C. (2000). The Relationship between geology and landslide hazards of Atchison, Kansas, and vicinity. Midcontinent Geoscience, 1-16.

Ohta, K., Kobashi, G., Takano, S., Kagaya, S., Yamada, H., Minakami, H., & Yamamura, E. (2007). Analysis of the geographical accessibility of neurosurgical emergency hospitals in Sapporo city using GIS and AHP. International Journal of Geographical Information Science, 21(6): 687-698.

Pachauri, A. K., Gupta, P. V., & Chander, R. (1998). Landslide zoning in a part of the Garhwal Himalayas. Environmental Geology, 36(3-4): 325-334.

Pandey, V. K., Pourghasemi, H. R., & Sharma, M. C. (2020). Landslide susceptibility mapping using maximum entropy and support vector machine models along the Highway Corridor, Garhwal Himalaya. Geocarto International, 35(2): 168-187.

Park, N. W. (2015). Using maximum entropy modeling for landslide susceptibility mapping with multiple geoenvironmental data sets. Environmental Earth Sciences, 73(3): 937-949.

Parteli, E. J. R., Schmidt, J., Blümel, C., Wirth, K.-E., Peukert, W. & Pöschel, T. (2014). Attractive particle interaction forces and packing density of fine glass powders. Scientific Reports, 4(1): 1-7.

Pearce, J. & Ferrier, S. (2000) Evaluating the predictive performance of habitat models developed using logistic regression. Ecological Modelling, 133: 225 –245.

Peng, L., Niu, R., Huang, B., Wu, X., Zhao, Y., & Ye, R. (2014). Landslide susceptibility mapping based on rough set theory and support vector machines: A case of the Three Gorges area, China. Geomorphology, 204: 287-301.

Peterson, A.T., Ball, L.G. & Cohoon, K.P., (2002a). Predicting distributions of Mexican birds using ecological niche modelling methods. Ibis, 144(1): 27-32.

Pham, B. T., Bui, D. T., & Prakash, I. (2018). Bagging based Support Vector Machines for spatial prediction of landslides. Environmental Earth Sciences, 77(4): 146.

Phillips, S. J., Anderson, R. P., & Schapire, R. E. (2006). Maximum entropy modeling of species geographic distributions. Ecological Modelling, 190(3-4): 231-259.

Phillips, S. J., Dudík, M., & Schapire, R. E. (2004, July). A maximum entropy approach to species distribution modeling. In Proceedings of the twenty-first international conference on Machine learning (p. 83). ACM.

Phillips, S.J. & Dudı´k, M. (2008) Modeling of species distributions with Maxent: new extensions and a comprehensive evaluation. Ecography, 31: 161–175.

Phillips, S.J., Dudı´k, M., Elith, J., Graham, C.H., Lehmann, A., Leathwick, J. & Ferrier, S. (2009) Sample selection bias and presence-only distribution models: implications for background and pseudo-absence data. Ecological Applications, 19: 181–197.

Pontius Jr, R. G., & Schneider, L. C. 2001. Land-cover change model validation by a ROC method for the Ipswich watershed, Massachusetts, USA. Agriculture, Ecosystems & Environment, 85(1-3): 239-248.

Pourghasemi, H. R., & Kerle, N. (2016). Random forests and evidential belief function-based landslide susceptibility assessment in Western Mazandaran Province, Iran. Environmental Earth Sciences, 75(3):185.

Pourghasemi, H. R., Jirandeh, A. G., Pradhan, B., Xu, C. & Gokceogluet, C. (2013). Landslide susceptibility mapping using support vector machine and GIS at the Golestan Province, Iran. Journal of Earth System Sciences 122:349–369.

Pourghasemi, H. R., Kariminejad, N., Amiri, M., Edalat, M., Zarafshar, M., Blaschke, T. & Cerda, A. (2020). Assessing and mapping multi-hazard risk susceptibility using a machine learning technique. Scientific Reports,10: 3203.

Pourghasemi, H. R., Pradhan, B., & Gokceoglu, C. (2012). Application of fuzzy logic and analytical hierarchy process (AHP) to landslide susceptibility mapping at Haraz watershed, Iran. Natural Hazards, 63(2): 965-996.

Pradhan, B., Sezer, E. A., Gokceoglu, C., & Buchroithner, M. F. (2010). Landslide susceptibility mapping by neuro-fuzzy approach in a landslide-prone area (Cameron Highlands, Malaysia). IEEE Transactions on Geoscience and Remote Sensing, 48(12): 4164-4177.

Radbruch-Hall, D. H., & Varnes, D. J. (1976). Landslides—cause and effect. Bulletin of the International Association of Engineering Geology-Bulletin de l'Association Internationale de Géologie de l'Ingénieur, 13(1): 205-216.

Rahmati, O., Golkarian, A., Biggs, T., Keesstra, S., Mohammadi, F., & Daliakopoulos, I. N. (2019). Land subsidence hazard modeling: Machine learning to identify predictors and the role of human activities. Journal of Environmental Management, 236: 466-480.

Reichenbach, P, Mondini, A. & Rossi, M. (2014). The influence of land use change on landslide susceptibility zonation: the Briga catchment test site (Messina, Italy). Environmental Management, 54(6): 1372-1384.

Remondo, J., Bonachea, J., & Cendrero, A. (2008). Quantitative landslide risk assessment and mapping on the basis of recent occurrences. Geomorphology, 94(3-4): 496-507.

Roodposhti, M. S., Rahimi, S., & Beglou, M. J. (2014). PROMETHEE II and fuzzy AHP: an enhanced GIS-based landslide susceptibility mapping. Natural Hazards, 73(1): 77-95.

Roy, J., & Saha, S. (2019). Landslide susceptibility mapping using knowledge driven statistical models in Darjeeling District, West Bengal, India. Geoenvironmental Disasters, 6(1): 11.

Saaty, T. L. (1977). A scaling method for priorities in hierarchical structures. Journal of Mathematical Psychology, 15(3): 234-281.

Salarian, T., Zare, M., Jouri, M. H., Miarrostami, S., & Mahmoudi, M. (2014). Evaluation of shallow landslides hazard using artificial neural network of Multi-Layer Perceptron method in Subalpine Grassland (Case study: Glandrood watershed-Mazandaran). International Journal of Agriculture and Crop Sciences, 7(11): 795.

Sánchez-Flores, E. (2007). GARP modeling of natural and human factors affecting the potential distribution of the invasives Schismus arabicus and Brassica tournefortii in ‘El Pinacate y Gran Desierto de Altar’Biosphere Reserve. Ecological Modelling, 204(3-4): 457-474.

Schmidt, J., Parteli, E. J. R., Uhlmann, N., Wörlein, N., Wirth, K.-E., Pöschel, T. & Peukert, W. (2020). Packings of micron-sized spherical particles - insights from bulk density determination, X-ray microtomography and discrete element simulations. Advanced Powder Technology 31: 2293-2304.

Schneiderbauer, S., & Ehrlich, D. (2004). Risk, hazard and people’s vulnerability to natural hazards. A review of definitions, concepts and data. European Commission Joint Research Centre. EUR, 21410: 40.

Sevgen, E., Kocaman, S., Nefeslioglu, H. A., & Gokceoglu, C. (2019). A novel performance assessment approach using photogrammetric techniques for landslide susceptibility mapping with logistic regression, ANN and random forest. Sensors, 19(18): 3940.

Shanmugam, G. & Wang, Y. (2015). The landslide problem. Journal of Palaeogeography. 4(2): 109-166.

Sharma, L. P., Patel, N., Ghose, M. K., & Debnath, P. (2013). Synergistic application of fuzzy logic and geo-informatics for landslide vulnerability zonation—a case study in Sikkim Himalayas, India. Applied Geomatics, 5(4): 271-284.

Sidle, R., & Ochiai, H. (2006). Processes, prediction, and land use. Water resources monograph. American Geophysical Union, Washington. 1-307.

Stockman, A. K., Beamer, D. A., & Bond, J. E. (2006). An evaluation of a GARP model as an approach to predicting the spatial distribution of non-vagile invertebrate species. Diversity and Distributions, 12(1): 81-89.

Stockwell, D. (1999). The GARP modelling system: problems and solutions to automated spatial prediction. International Journal of Geographical Information Science, 13(2): 143-158.

Stockwell, D. R., & Noble, I. R. (1992). Induction of sets of rules from animal distribution data: a robust and informative method of data analysis. Mathematics and Computers in Simulation, 33(5-6): 385-390.

Suzen, M. L., Doyuran, V., (2004a). A comparison of the GIS based landslide susceptibility assessment methods: multivariate versus bivariate. Environ Geol, 45:665-679.

Suzen, M. L., Doyuran, V., (2004b). Data driven bivariate landslide susceptibility assessment using geographical information systems: a method and application to Asarsuyu catchment, Turkey, Eng. Geol., 71:303-352.

Taxonomy, S. (2003). Soil survey staff. Keys to Soil Taxonomy. USDA, Ninth Edition, 332p.

Tazik, E., Jahantab, Z., Bakhtiari, M., Rezaei, A., & Alavipanah, S. K. (2014). Landslide susceptibility mapping by combining the three methods fuzzy logic, frequency ratio and analytical hierarchy process in Dozain basin. The International Archives of Photogrammetry, Remote Sensing and Spatial Information Sciences, 40(2): 267.

Tobin, G.A. & Montz, B.E., (1997). Natural Hazards: Explanation and Integration. The Guilford Press, New York, 388p.

Tourani, M., Caglayan, A., Saber, R., Isik, V. (2021). Determination of Land Subsidence in Gorgan Plain with Insar Method (Golestan, NE Iran). In book: Geoscience for Society, Education and Environment. Chapter: 3.11. Publisher: Romanian Society of Applied Geophysics (SGAR).

Townsend Peterson, A., Papeş, M., & Eaton, M. (2007). Transferability and model evaluation in ecological niche modeling: a comparison of GARP and Maxent. Ecography, 30(4): 550-560.

Uzielli, M., Nadim, F., Lacasse, S., & Kaynia, A. M. (2008). A conceptual framework for quantitative estimation of physical vulnerability to landslides. Engineering Geology, 102(3-4): 251-256.

Vahidnia, M. H., Alesheikh, A. A., Alimohammadi, A., & Hosseinali, F. (2010). A GIS-based neuro-fuzzy procedure for integrating knowledge and data in landslide susceptibility mapping. Computers & Geosciences, 36(9): 1101-1114.

Vakhshoori, V., Pourghasemi, H. R., Zare, M., & Blaschke, T. (2019). Landslide Susceptibility Mapping Using GIS-Based Data Mining Algorithms. Water, 11(11): 2292.

Van Den Eeckhaut, M., Hervás, J., Jaedicke, C., Malet, J. P., Montanarella, L., & Nadim, F. (2012). Statistical modelling of Europe-wide landslide susceptibility using limited landslide inventory data. *Landslides*, *9*(3): 357-369.

van Westen, C. J., Van Asch, T.W.J., Soeters, R., (2005). Landslide hazard and risk zonation; why is it still so difficult? Bulletin of Engineering geology and the Environment 65 (2): 167-184.

Vapnik, V.N., (1999). The Nature of Statistical Learning Theory. Second Edition, Springer Verlag, New York, 314p.

Varnes, D. J., (1984). Landslide hazard zonation: a review of principles and practice. The UNESCO Press, Paris, No 3, 63 pp.

Wang, H., Zhang, J., & Lin, H. (2019). Satellite-based analysis of landfill landslide: the case of the 2015 Shenzhen landslide. International Journal of Geotechnical Engineering, 1-8.

Wang, S., Xu, Q., & Luo, B. (2017). Vulnerability analysis and susceptibility evaluation of landslides based on fractal theory in Nanjiang County. Hydrogeol Eng Geol, 44(3): 119-126.

Wang, X. Y., Huang, X. L., Jiang, L. Y., & Qiao, G. X. (2010). Predicting potential distribution of chestnut phylloxerid (Hemiptera: Phylloxeridae) based on GARP and Maxent ecological niche models. Journal of Applied Entomology, 134(1): 45-54.

Wang, Y., Xie, B., Wan, F., & Xiao, Q. (2007). Application of ROC curve analysis in evaluating the performance of alien species' potential distribution models. Biodiversity Science, 15(4): 365-372.

Xiao, L., Zhang, Y., & Peng, G. (2018). Landslide susceptibility assessment using integrated deep learning algorithm along the China-Nepal highway. *Sensors*, *18*(12):4436.

Yalcin, A. (2008). GIS-based landslide susceptibility mapping using analytical hierarchy process and bivariate statistics in Ardesen (Turkey): comparisons of results and confirmations. Catena, 72(1): 1-12.

Yao, X., Tham, L. G., & Dai, F. C. (2008). Landslide susceptibility mapping based on support vector machine: a case study on natural slopes of Hong Kong, China. Geomorphology, 101(4): 572-582.

Yesilnacar, E., & Topal, T. (2005). Landslide susceptibility mapping: a comparison of logistic regression and neural networks methods in a medium scale study, Hendek region (Turkey). Engineering Geology, 79(3-4): 251-266.

Yesilnacar, E.K. (2005). The application of computational intelligence to landslide susceptibility mapping in Turkey. University of Melbourne, Department, 200.

Youssef, A. M., Pourghasemi, H. R., Pourtaghi, Z. S., & Al-Katheeri, M. M. (2016). Landslide susceptibility mapping using random forest, boosted regression tree, classification and regression tree, and general linear models and comparison of their performance at Wadi Tayyah Basin, Asir Region, Saudi Arabia. Landslides, 13(5): 839-856.

Zêzere, J. L., Garcia, R. A. C., Oliveira, S. C., & Reis, E. (2008). Probabilistic landslide risk analysis considering direct costs in the area north of Lisbon (Portugal). Geomorphology, 94(3-4): 467-495.

Zhao, T., Dai, F., & Xu, N. W. (2017). Coupled DEM-CFD investigation on the formation of landslide dams in narrow rivers. Landslides, 14(1): 189-201.

Zhu, L., Sun, O. J., Sang, W., Li, Z., & Ma, K. (2007). Predicting the spatial distribution of an invasive plant species (Eupatorium adenophorum) in China. Landscape Ecology, 22(8): 1143-1154.

Zhuang, J., Cui, P., Hu, K., Chen, X. & Yonggang, G. E. (2010). Characteristics of earthquake-triggered landslides and post-earthquake debris flows in Beichuan County. Journal of Mountain Science.7: 246–254.